Topo-bathymetric Lidar Research to support Remediation of Boat Harbour

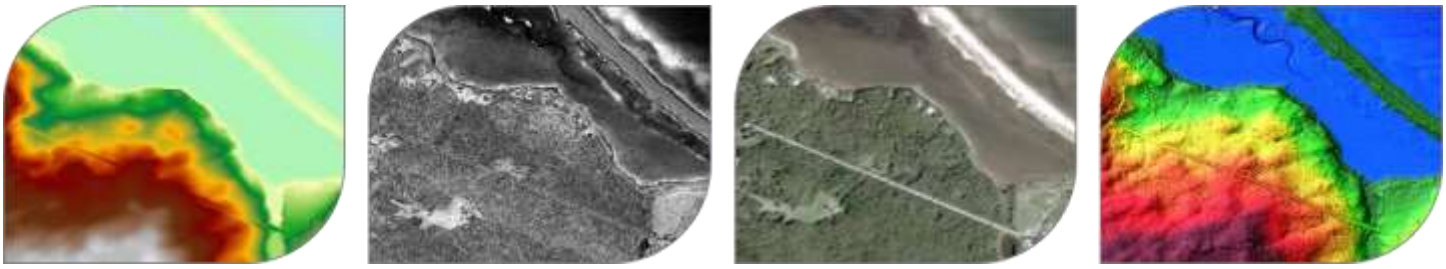

Prepared by

Applied Geomatics Research Group
NSCC, Middleton
Tel. 902 825 5475
email: tim.webster@nscc.ca

Submitted to

Public Services and Procurement Canada
March 31st, 2017

How to cite this work and report:

Webster, T., Collins, K., Vallis, A. 2017. “Topo-Bathymetric Lidar Research to support remediation of Boat Harbour” Technical report, Applied Geomatics Research Group, NSCC Middleton, NS.

Executive Summary

The Applied Geomatics Research Group (AGRG) surveyed outer Pictou Harbour using airborne topo-bathymetric lidar in September 2016 to collect high-resolution elevation data and imagery. The sensor used was AGRG's Chiroptera II integrated topo-bathymetric lidar system, equipped with a 60 megapixel (MPIX) multispectral camera.

Boat Harbour is currently acting as a holding facility for effluent from the nearby Abercrombie Point Pulp Mill, but there is a plan to remediate this area back to its original state, as a tidal inlet. One of the objectives of this project was to develop a hydrodynamic model to simulate baseline current flow, water level variations and water circulation within outer Pictou Harbour. The hydrodynamic model was validated by comparing modelled surface elevation, and current speed and direction to observations from an Acoustic Doppler Current Profiler, which was deployed for 35 days to measure the water level and current speeds throughout a tidal cycle. The modelled surface elevation agreed very well with the observed surface elevation. The modelled east-west currents agreed well with the phase of the observations, but the model did not consistently simulate the observed variation in amplitude between tides. The model captured the large-scale nature of the north-south currents, predicting the amplitude of the flood tide well but predicting the phase wrong, and modelling some of the finer signals of the southern ebb tide well in phase but under-predicting amplitude. Current speed was highest in and near the Pictou Harbour channel, reaching 0.5 m/s along the axis of the channel, and currents near the outlet of Boat Harbour were slower, approximately 0.01 m/s during maximum ebb and flood flow.

In addition to the HD model, baseline information on the geomorphology and ecology of Pictou Harbour was also an objective of the study. The topo-bathymetric data and derived products (hydrodynamic model, imagery, digital elevation and surface models, lidar seabed reflectance, bottom type map) provide a detailed reference of the coastal environment and ecology, as part of the deliverables for this project. The plume discharging out of Boat Harbour was clearly visible on the imagery and the lidar did not penetrate through this dark mass of water. The bottom type classification depicting eelgrass distribution along with other cover types was produced from the data collected during the lidar survey is in very good agreement with the ground truth points collected. These data will help to determine if Pictou Harbour changes when Boat Harbour is converted back to its natural setting as a tidal inlet. One should consider a mapping program to measure the natural variability of the physical and biological system before Boat Harbour is altered, then a systematic mapping program to measure change once it is altered. AGRG researchers collected survey grade GPS points, water clarity, depth and underwater photos of the seabed conditions and bottom type. A bottom type classification map was produced from the lidar and photo products that separated bottom type into eelgrass, focus, mud, and sand. Fucus and sand were identified correctly by the classification 100% of the time, eelgrass 87.5% of the time, and mud 25% of the time.

Table of Contents

Table of Figures

List of Tables

1 Introduction

1.1 Project Background

With the construction of a pulp mill at Abercrombie Point in 1967, Boat Harbour was transformed from a tidal inlet to a holding facility for effluent from the mill. A plan is in place to remediate Boat Harbour in an attempt to return it back to its original state. With the change back to a tidal inlet, the surrounding coastline in Pictou Harbour may change because of the changes in water circulation. It is important to capture a baseline of the current state of the coastal environment and the ecological distribution of materials.

The Applied Geomatics Research Group (AGRG) of the Nova Scotia Community College (NSCC) has many years of experience with lidar technology and coastal mapping. Recently the NSCC has acquired a topo-bathymetric lidar sensor and high-resolution aerial camera that is capable of surveying both the land topography and the submerged coastal topography, or bathymetry. This new topo-bathymetric lidar sensor offers a unique method to survey the shoreline in more detail than present, map and characterize environmentally sensitive areas, use the nearshore bathymetry to model the local tidal currents, and chart nearshore hazards to navigation.

In the summer of 2016, AGRG used the lidar system to survey Pictou Harbour. This report will highlight the results of the lidar survey and the derived data products, including the digital elevation model (DEM), digital surface model (DSM), and lidar intensity model, all derived from the lidar point cloud. Additionally, this report will present the high-resolution RCD30 60 MPIX imagery, processed using the aircraft trajectory and direct georeferencing. Ground truth maps, included in this report will highlight the results of the ground truth survey such as bottom type, seagrass percentage and water clarity. For the intertidal and subtidal areas this level of information has never been surveyed before with such sophisticated equipment and provides a rich series of GIS-ready data layers for capturing the baseline information for this study. The bathymetry from the survey was used to construct a hydrodynamic model of the circulation within outer Pictou Harbour based on present day conditions.

In addition to the deliverables stated above, the data collected from a nearby location, Little Harbour, surveyed and studied by AGRG in 2014 will be delivered. The DEM, airphoto mosaic, and eelgrass map can be used by NS Lands as a reference area, to provide a picture of what Boat Harbour may look like when converted back to its natural setting.

1.2 Study Area

Boat Harbour is located on the Nova Scotia shoreline of the Northumberland Strait, in Pictou County (Figure 1-1). The study area is east of Pictou Harbour and the Abercrombie Point Pulp Mill, and encompasses the community of Pictou Landing. The geography of this study area renders it a tidal inlet; however, it is currently acting as a holding facility for effluent from the pulp mill.

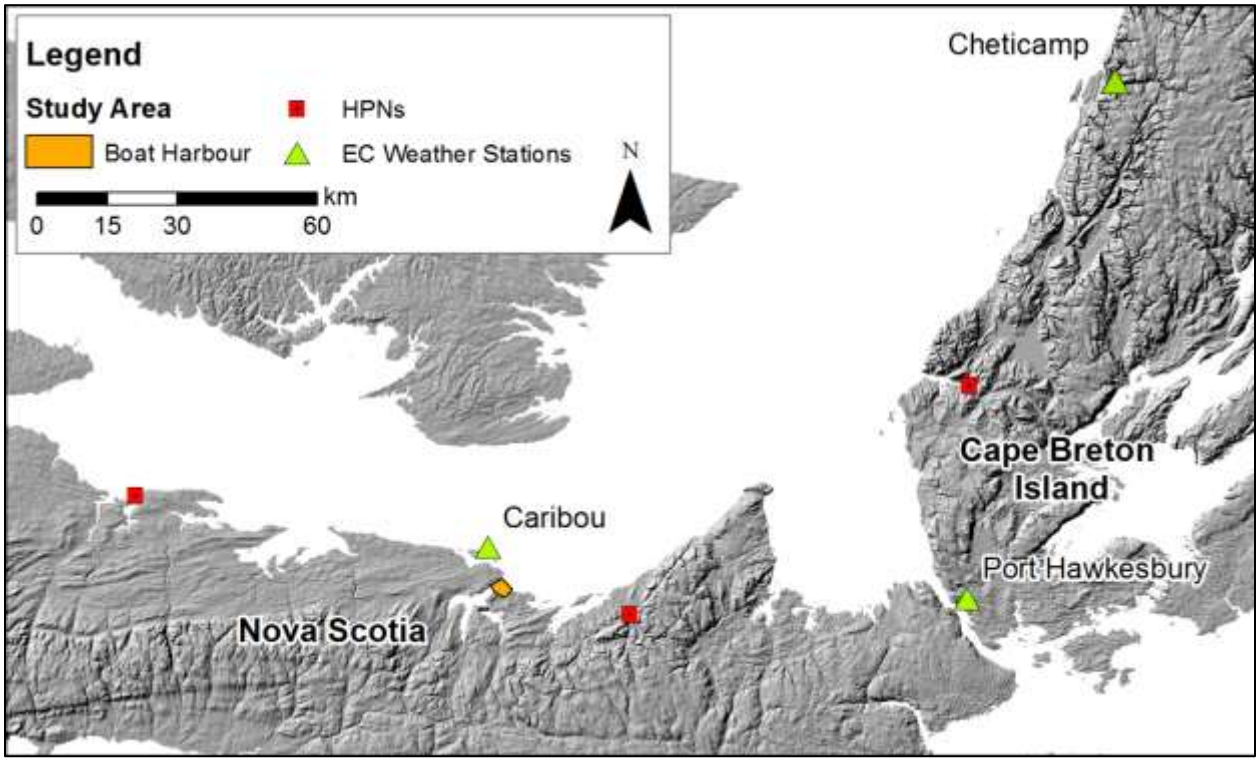

Figure 1-1: The topographic-bathymetric lidar study area in the Southern Gulf of St. Lawrence. Shown is the Boat Harbour study area (gold polygon), NS High Precision Network (HPN) stations (orange squares) and Environment Canada (EC) Weather Stations (green triangles).

2 Methods

2.1 Sensor Specifications

The AGRG utilized the Chiroptera II integrated topographic-bathymetric lidar sensor equipped with a 60 MPIX multispectral camera for this study. The system incorporates a 1064 nm near-infrared laser for ground returns and sea surface and a green 515 nm laser for bathymetric returns (Figure 2-1, Figure 2-2d). The lasers scan in an elliptical pattern, which enables coverage from many different angles on vertical faces, causes less shadow effects in the data, and is less sensitive to wave interaction. The bathymetric laser is limited by depth and clarity, and has a depth

penetration rating of roughly 1.5 x the Secchi depth (a measure of turbidity or water clarity using a black and white disk). The Leica RCD30 camera (Figure 2-2d) collects co-aligned RGB+NIR motion compensated photographs which can be mosaicked into a single image in post-processing, or analyzed frame by frame for maximum information extraction. For the purposes of this report, the topographic laser will be referred to as the “topo” laser, and the bathymetric laser will be referred to as the ”bathy” laser.

The calibration of the lidar sensor and camera have been documented in an external report which will be included as part of the deliverables for this project.

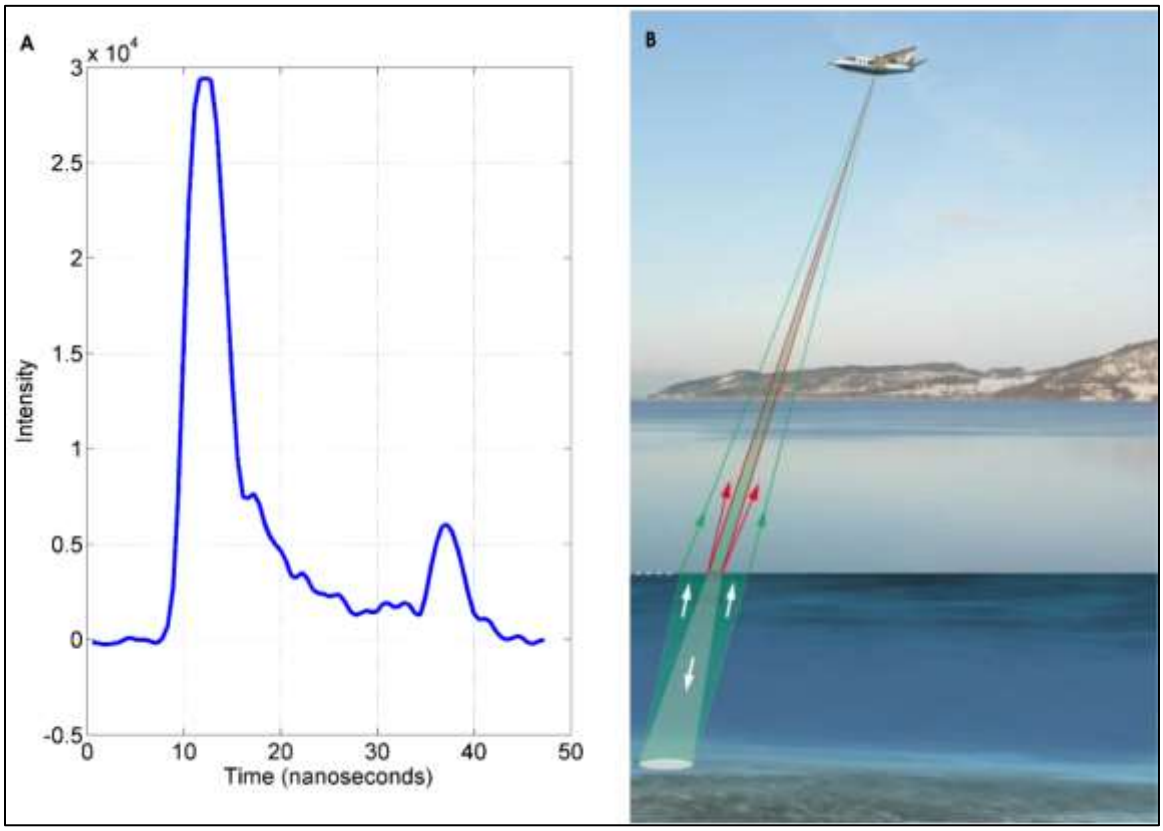

Figure 2-1: (A) Example of the Chiroptera II green laser waveform showing the large return from the sea surface and smaller return from the seabed. (B) Schematic of the Chiroptera II green and NIR lasers interaction with the sea surface and seabed (adapted from Leica Geosystems).

Figure 2-2: (a) Aircraft used for 2016 lidar survey; (b) display seen by lidar operator in-flight; (c) main body of sensor (right) and the data rack(left); (d) large red circles are the lasers; the RCD30 lens (right) and low resolution camera quality control(left).

2.2 Lidar Survey Details

The lidar survey was conducted in Sept 2016 (Table 1). The surveys were planned using Mission Pro software. The 19 planned flight lines for Boat Harbour are shown in Figure 2-3. The aircraft required ground-based high precision GPS data to be collected during the lidar survey in order to provide accurate positional data for the aircraft trajectory. Our Leica GS14 RTK GPS system was used to set up a base station set to log observations at 1-second intervals over a Nova Scotia High Precision Network (HPN) (Figure 1-1).

Survey Date	Survey Time (UTC)	Survey Duration	Number of Flight Lines
Sept 7	13:15 – 14:50	1 hour 35 mins	19

Table 1: 2016 NS Lands lidar survey dates, durations, areas, and flight lines.

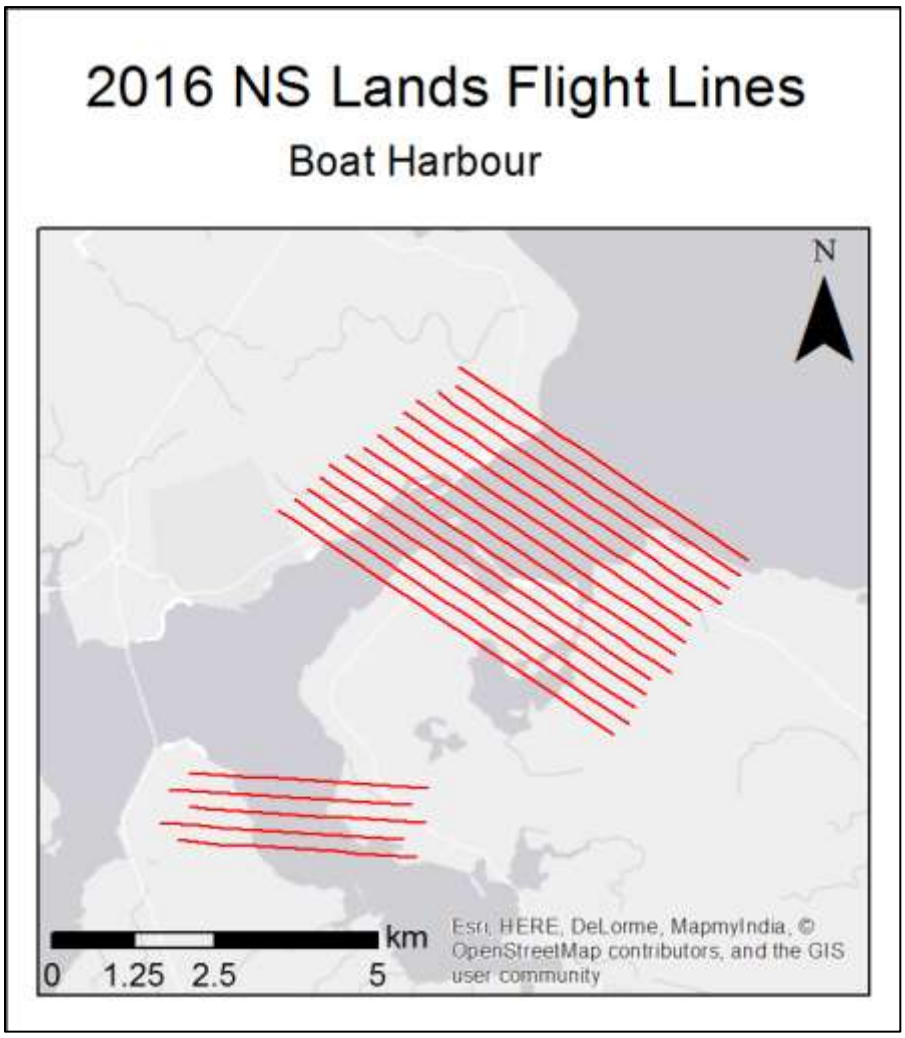

Figure 2-3: Flight lines for 2016 lidar survey in Boat Harbour.

2.3 Ground Truth Data Collection

Ground truth data collection is a crucial aspect of topo-bathymetric lidar surveys. In August 2016, AGRG researchers conducted traditional ground truth data collection including hard surface validation and depth measurements to validate the lidar, Secchi depth measurements for information on water clarity, and underwater photographs to obtain information

on bottom type and vegetation. (Figure 2-5) The seabed elevation was measured directly using a large pole onto which the RTK GPS was threaded, in addition to manual measurements using a depth mate consisting of a lead ball on a graduated rope, in addition to a commercial-grade single beam echo sounder. By threading the RTK GPS antenna on the pole and measuring the elevation of the seabed directly we eliminated errors introduced into depth measurements obtained from a boat such as those caused by wave action, tidal variation, and angle of rope for lead ball drop measurements. Table 2 summarizes the ground truth measurements undertaken for the Boat Harbour study area in 2016, and Figure 2-4 shows a map of the distribution of ground truth measurements. Figure 2-5 illustrates some of the ground truth collection and results at Boat Harbour.

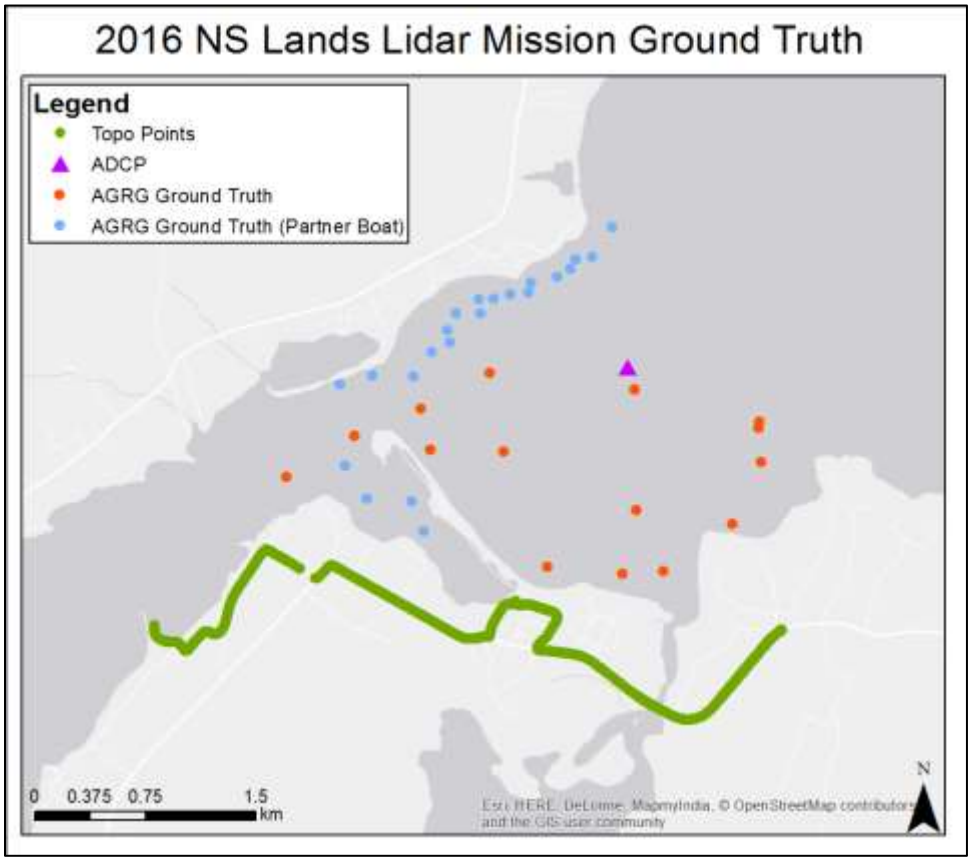

Figure 2-4: Location of hard surface GPS validation points, AGRG and partner boat-based ground truth points, and ADCP deployment at Boat Harbour.

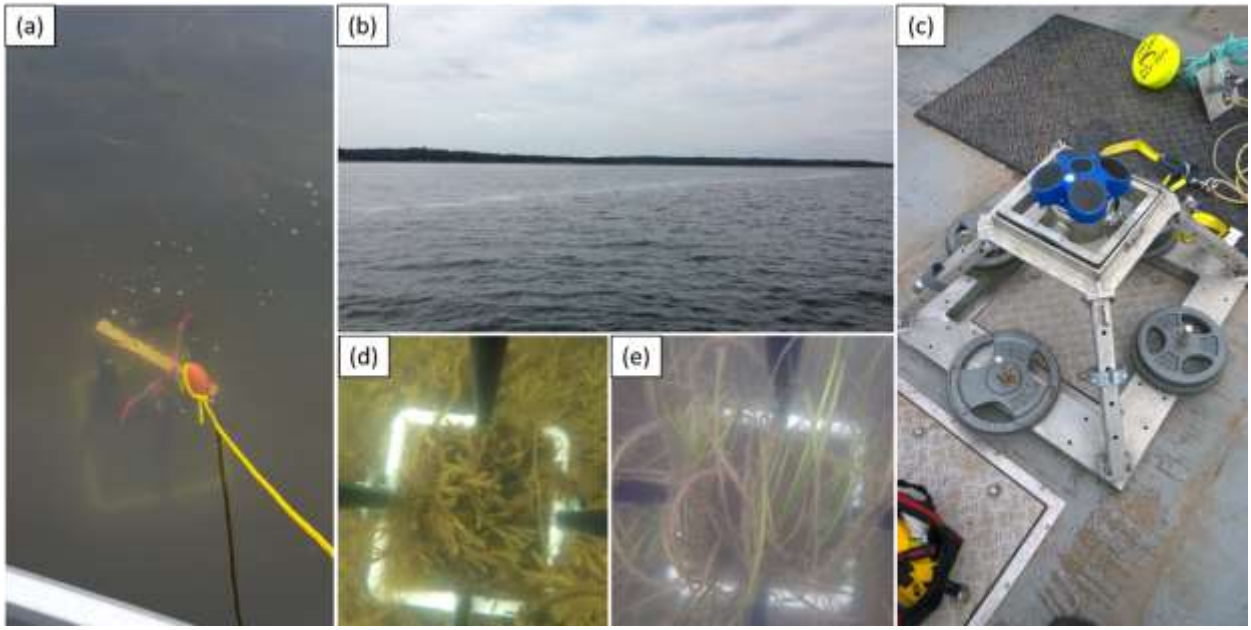

Figure 2-5: Ground truth collection at Boat Harbour. (a) Submerged quadrat collecting ground truth imagery, (b) Plume in Boat Harbour, (c) ADCP deployment, (d) and (e) Ground truth imagery results from quadrat.

Date	Base station (id)	GPS System (GS14 or 530/1200)	Secchi (Y or -)	Depth (see caption for options)	ADCP (Deployed, -, or Retrieved)	Underwater Photos (see caption for options)	Hard Surface GPS (Y or -)	CTD (Y or -)	Turbidity Buoy (deployed and recovered)	Cube (deployed and recovered)	River Ray (Y or -)
Aug 11	206392	GS14, 1200	Y	P, M, DM	Deployed	Q_{50}	Y	-	-	-	-
Aug 30	-	GS14	-	-	-	-	-	-	-	-	Y
Sept 13	-	-	-	-	Recovered	-	-	-	-	-	-

Table 2: Ground truth data summary. GPS Column: Two Leica GPS systems were used, the GS14 and the 1200. Depth Column: P=GPS antenna threaded onto the large pole for direct bottom elevation measurement; M=manual depth measurement using lead ball or weighted Secchi disk; DM=handheld single beam DepthMate echo sounder. Underwater Photos: Q_{50}=0.25 m^2 quadrat with downward-looking GoPro camera.

2.4 Time of Flight Conditions: Weather, Tide and Turbidity

Meteorological conditions during and prior to topo-bathy lidar data collection are an important factor in successful data collection. As the lidar sensor is limited by water clarity, windy conditions have the potential to stir up any fine sediment in the water and prevent laser penetration. Rain is not suitable for lidar collection, and the glare of the sun must also be factored in for the collection of aerial photography. Before each lidar survey we primarily monitored weather forecasts using four tools: the Environment Canada (EC) public forecast (http://weather.gc.ca/) (Figure 1-1); EC's Marine Forecast (https://weather.gc.ca/marine/index_e.html); SpotWx (www.spotwx.com), which allows the user to enter a precise location and choose from several forecasting models of varying model resolution and forecast length; and a customized EC forecast for the lidar study area provided to AGRG every eight hours. Each of these tools had strengths and weaknesses and it was through monitoring all four that a successful lidar mission was achieved. For example, the customized EC forecast was the only tool that provided a fog prediction, on an hourly basis. However, the SpotWx graphical interface proved superior for wind monitoring. Only the EC public forecast alerted us to Weather Warnings that were broadcast in real-time, such as thunderstorms, and the marine forecast provided the only information for offshore conditions.

Although the summer of 2016 was particularly hot and dry, a suitable window for the Pictou Harbour lidar survey was not available until Sept. 7. The survey followed three days of <20 km/h winds blowing mainly from the south; there were

no major rainfall events in the week before the survey, which could have caused the water clarity to be reduced, and the survey started following low tide and ended at mid-tide (Figure 2-6).

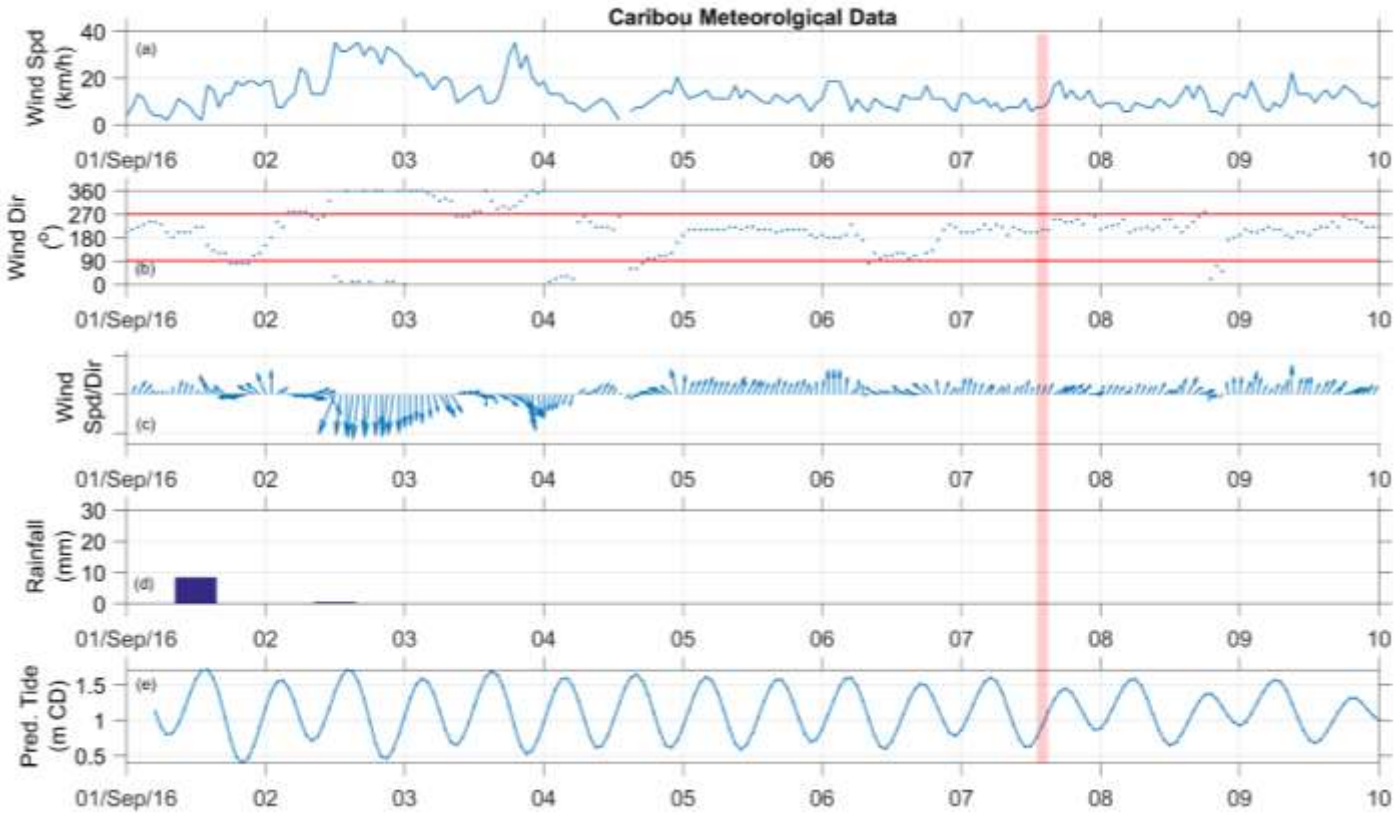

Figure 2-6: (a) Wind speed and (b) direction collected at the EC weather station at Caribou between Sept. 1 and 10, 2016, at 1 hour intervals. Panel (c) shows a vector plot of the wind, where the arrows point in the direction the wind is blowing, and the red box indicates the lidar survey duration. Panel (d) shows daily rainfall and (e) shows predicted tide at Pictou Harbour.

2.5 Acoustic Doppler Current Profiler (ADCP)

A Teledyne RDI Sentinel V20 1000 kHz Acoustic Doppler Current Profiler (ADCP) was deployed at Boat Harbour on August 11th to measure current speed and direction for minimum 35 days. The ADCP was recovered on September 13th. The current data were obtained for hydrodynamic model validation. Surface elevation of the ADCP compared well to CHS predicted tides and tidal range was 1.7 m (Figure 2-7). The current at the ADCP was dominated by tidal circulation and ranged from -0.24 m/s to 0.28 m/s in the east-west direction, and from -0.33 m/s to 0.06 m/s in the north-south direction (Figure 2-8). The vertical structure and magnitude of the currents varied throughout the tidal cycle, with the strongest currents occurring during the middle of the deployment when the tide was semidiurnal, near the water surface (Figure 2-9). When the tide was mixed, semidiurnal the currents were weaker during the lower tidal range and stronger during the higher tidal range (Figure 2-10).

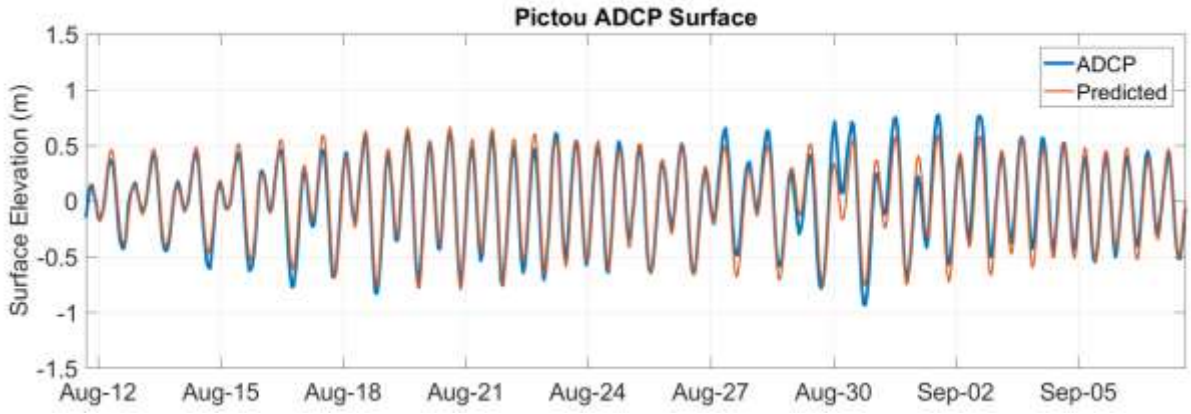

Figure 2-7: ADCP and CHS predicted surface elevation during the ADCP deployment.

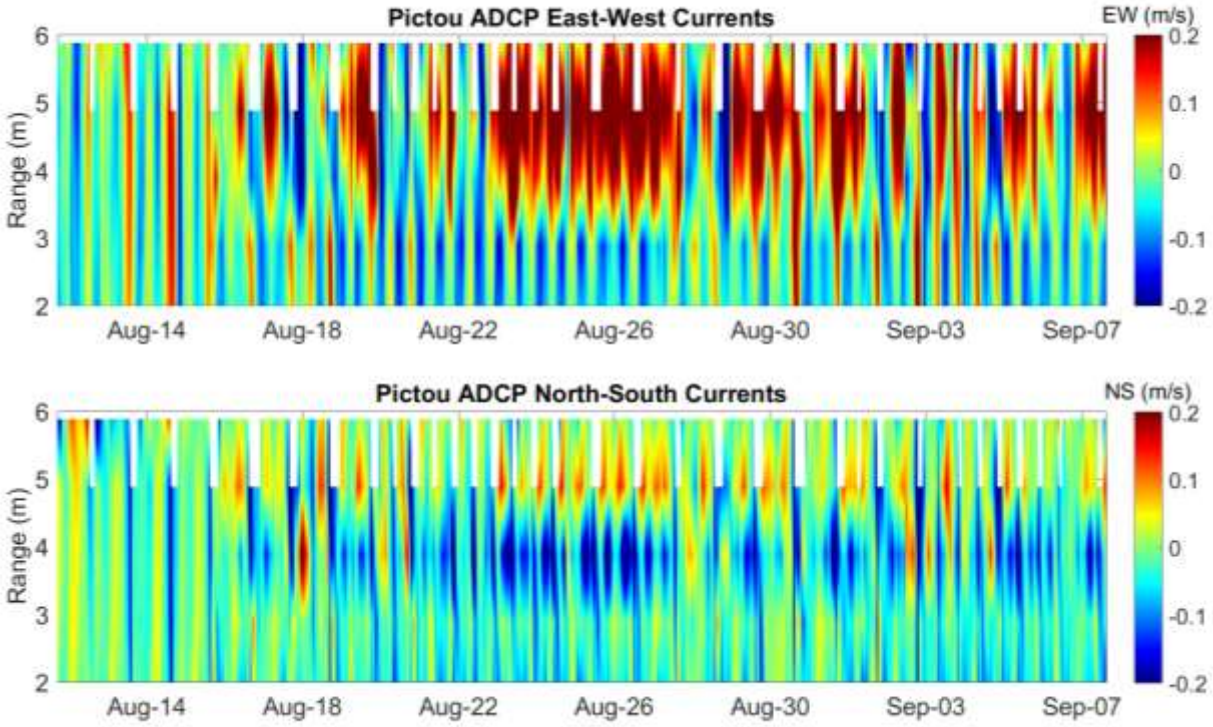

Figure 2-8: Current speeds over time (x axis) and depth (y axis, measured as range from the ADCP) for East-West currents (top panel) and North-South currents (bottom panel). Colours indicate current magnitude and direction.

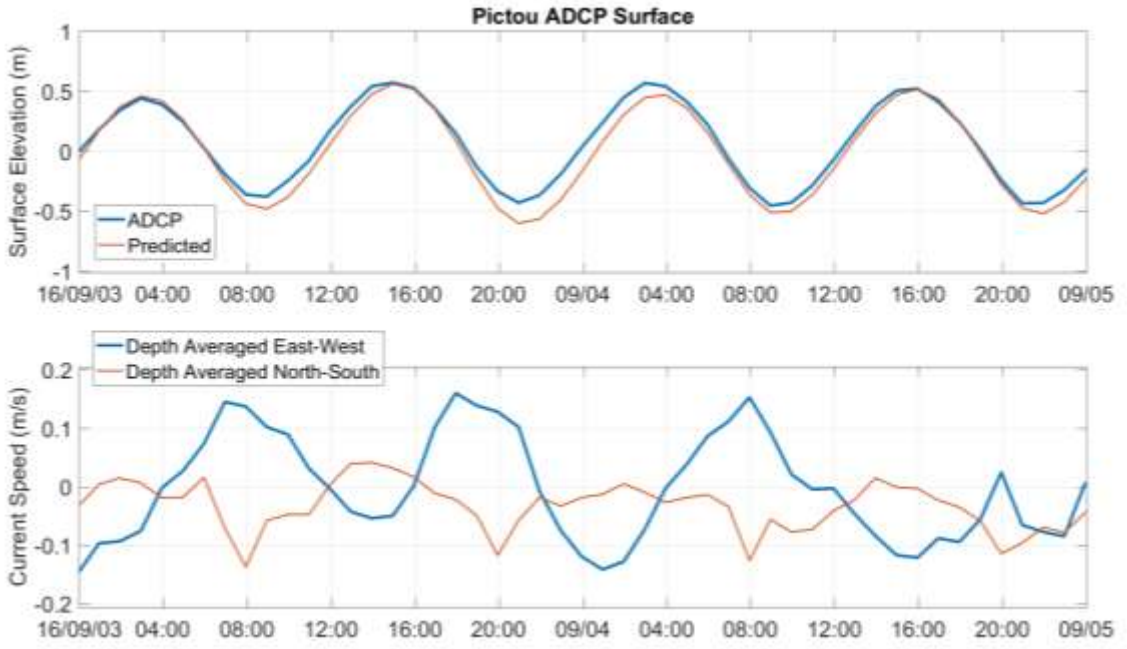

Figure 2-9: Observed and predicted surface elevation (top panel) and depth averaged currents (lower panel) between Sept. 3 and 5 during a semidiurnal tidal phase.

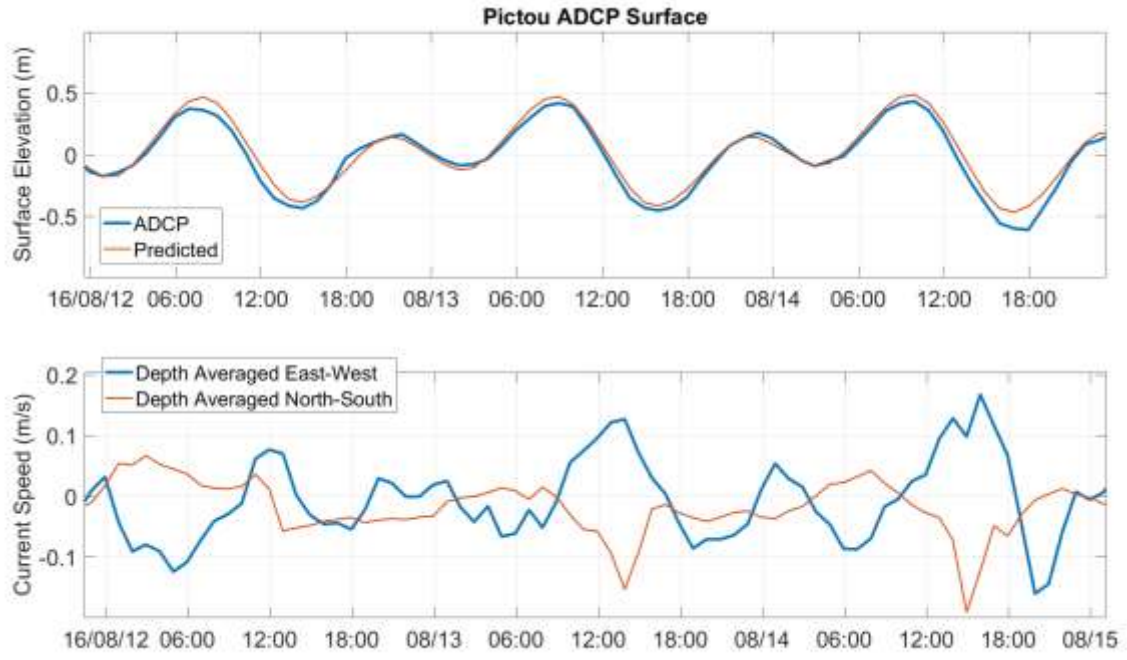

Figure 2-10: Observed and predicted surface elevation (top panel) and depth averaged currents (lower panel) between Aug. 12 - 15 during a mixed semidiurnal tidal phase.

2.6 Elevation Data Processing

2.6.1 Lidar processing

2.6.1.1 Point Cloud Processing

Once the GPS trajectory was processed for the aircraft, GPS observations were combined with the inertial measurement unit and the navigation data was linked to the laser returns and georeferenced. Lidar Survey Studio (LSS) software accompanies the Chiroptera II sensor and is used to process the lidar waveforms into discrete points. These data can then be inspected to ensure sufficient overlap between flight lines (30%) and that no gaps existed in the lidar coverage.

Integral to the processing of bathymetric lidar is the ability to map the water surface. The defined water surface is critical for two components of georeferencing the final target or targets that the reflected laser pulse recorded: the refraction of the light when it passes from the medium of air to water and the change in the speed of light from air to water. The LSS software computes the water surface from the lidar returns of both the topo and bathy lasers. In addition to classifying points as land, water surface or bathymetry, the system also computes a water surface that ensures the entire area of water surface is covered regardless of the original lidar point density. As previously mentioned, part of the processing involves converting the raw waveform lidar return time series into discrete classified points using LSS signal processing. Waveform processing may include algorithms specific to classifying the seabed. The points were examined in LSS both in planimetric and cross-section views. The waveforms for each point can be queried so that the location of the waveform peak can be identified and the type of point defined, for example water surface and bathymetry.

The LAS files, the file type output from LSS, were then read into TerraScan™ with the laser returns grouped by laser type so they could be easily separated, analyzed and further refined. Because of the differences in the lidar footprint between the topo and bathy lasers, the bathy point returns would be used to represent the water surface and both bathy and topo points would be used to represent targets on the land. See Table 3 and the attached Data Dictionary report for the classification codes for the delivered LAS 1.2 files. The refined classified LAS files were read into ArcGIS™ and a variety of raster surfaces at a 1 m spatial resolution were produced.

Class number	Description
0	Water model
1	Bathymetry (Bathy)
2	Bathy Vegetation
3	N/A
4	Topo laser Ground
5	Topo laser non-ground (vegetation & buildings)
6	Hydro laser Ground
7	Bathy laser non-ground
8	Water
9	Noise

10	Overlap Water Model
11	Overlap Bathy
12	Overlap Bathy Veg
13	N/A
14	Overlap Topo Laser Ground
15	Overlap Topo Laser Veg
16	Overlap Bathy Laser Ground
17	Overlap Bathy Laser Veg
18	Overlap Water
19	Overlap Noise

Table 3. Lidar point classification Codes and descriptions. Note that 'overlap' is determined for points which are within a desired footprint of points from a separate flight line; the latter of which having less absolute range to the laser sensor.

2.6.1.2 Gridded Surface Models

There are three main data products derived from the lidar point cloud. The first two are based on the elevation and include the Digital Surface Model (DSM), which incorporates valid lidar returns from vegetation, buildings, ground and bathymetry returns, and the Digital Elevation Model (DEM) which incorporates ground returns above and below the water line. The third data product is the intensity of the lidar returns, or the reflectance of the bathy laser. The lidar reflectance, or the amplitude of the returning signal from the bathy laser, is influenced by several factors including water depth, the local angle of incidence with the target, the natural reflectivity of the target material, the transmission power of the laser and the sensitivity of the receiver.

2.6.1.3 Depth Normalization of the Green Laser

The amplitude of the returning signal from the bathy laser provides a means of visualizing the seabed cover, and is influenced by several factors including water depth and clarity, the local angle of incidence with the target, the natural reflectivity of the target material, and the voltage or gain of the transmitted lidar pulse. The raw amplitude data are difficult to interpret because of variances as a result of signal loss due to the attenuation of the laser pulse through the water column at different scan angles. Gridding the amplitude value from the bathy laser results in an image with a wide range of values that are not compensated for depth and have significant differences for the same target depending on the local angle of incidence from flight line to flight line. As a result, these data are not suitable for quantitative analysis and are difficult to interpret for qualitative analysis. A process has been developed to normalize the amplitude data for signal loss in a recent publication (Webster et al., 2016). The process involved sampling the amplitude data from a location with homogeneous seabed cover (e.g., sand or eelgrass) over a range of depths. These data were used to establish a relationship between depth and the logarithm of the amplitude value. The inverse of this relationship was used with the depth map to adjust the amplitude data so that they could be interpreted without the bias of depth. A depth normalized amplitude/intensity image (DNI) was created for the study site using this technique that can be more consistently

interpreted for the seabed cover material. Note that this analysis considers only bathymetric lidar values and ignores any topographic elevation points.

2.6.1.4 Aerial Photo Processing

The RCD30 60 MPIX imagery was processed using the aircraft trajectory and direct georeferencing. The low altitude and high resolution of the imagery required that the lidar data be processed first to produce bare-earth digital elevation models (DEMs) that were used in the orthorectification process. The aircraft trajectory, which combines the GPS position and the IMU attitude information into a best estimate of the overall position and orientation of the aircraft during the survey is required for this process. This trajectory, which is linked to the laser shots and photo events by GPS based time tags, is used to define the Exterior Orientation (EO) for each of the RCD30 aerial photos acquired. The EO, which has traditionally been calculated by selecting ground control point (x, y, and z) locations relative to the air photo frame and calculating a bundle adjustment, was calculated using direct georeferencing and exploiting the high precision of the navigation system. The EO file defines the camera position (x, y, z) for every exposure as well as the various rotation angles about the x, y and z axis known as omega, phi and kappa. The EO file along with a DEM was used with the aerial photo to produce a digital orthophoto. After the lidar data were processed and classified into ground points, the lidar-derived DEM (above and below the water line) was used in the orthorectification process in Erdas Imagine software and satisfactory results were produced.

2.6.2 Ellipsoidal to Orthometric Height Conversion

The original elevation of any lidar product are referenced to the same elevation model as the GPS they were collected with. This model is a theoretical Earth surface known as the ellipsoid, and elevations referenced to this surface are in ellipsoidal height (GRS80). To convert them to orthometric height (OHt), which is height relative to the Canadian Geodetic Vertical Datum of 1928 (CGVD28), an offset must be applied. The conversions are calculated based on the geoid-ellipsoid separation model, HT2, from Natural Resources Canada.

2.7 Bottom Type Classification

The eelgrass map was derived from the lidar and orthophotos and included the water depth raster, derived from the DEM, lidar bottom reflectance intensity, and the true-color aerial photograph orthomosaic. The approach uses the red and green imagery bands, which were extracted from the true-color aerial photograph orthomosaic. Ratios of their differences and of their sums were added together and weighted by the interlaced lidar intensity data. The result is then normalized by the effects of depth. The resulting raster represents vegetation presence index, and was subject to a threshold procedure to result in a final shapefile of vegetation presence or absence. The procedure to produce the final SAV map involved

manual editing the shapefile using the RGB photos for interpretation, and included removing shadows created by overlapping trees in the imagery and clipping of the dataset to the relevant area.

2.8 Lidar Validation

Ground elevation measurements obtained using the RTK GPS system were used to validate the topographic lidar returns on areas of hard, flat surfaces. The GPS antenna was mounted on a vehicle and data were collected along roads within the study area, and points were collected manually along any wharves (green lines on Figure 2-4) present in the study area.

Boat-based ground truth data were used to validate the bathymetric lidar returns (blue and orange dots on Figure 2-4). Although various methods were used to measure depth during fieldwork, for this report only points measured using the large pole fitted with the RTK GPS antenna to directly measure the seabed elevation were used for the accuracy assessment; points that measured depth using sonar or a weighted rope were not considered at this time.

For both hard surface and boat-based GPS points, the differences in the GPS elevation and the lidar elevation (ΔZ) were calculated by extracting the lidar elevation from the DEM at the checkpoint and subtracting the lidar elevation from the GPS elevation. GPS points were subject to a quality control assessment such that the standard deviation of the elevation was required to be < 0.05 m.

3 Results

3.1 Lidar Validation

3.1.1 Topographic Validation

There were 635 data points collected along the roads with a calculated mean ΔZ of -0.14 m ± 0.04 m (Figure 3-1).

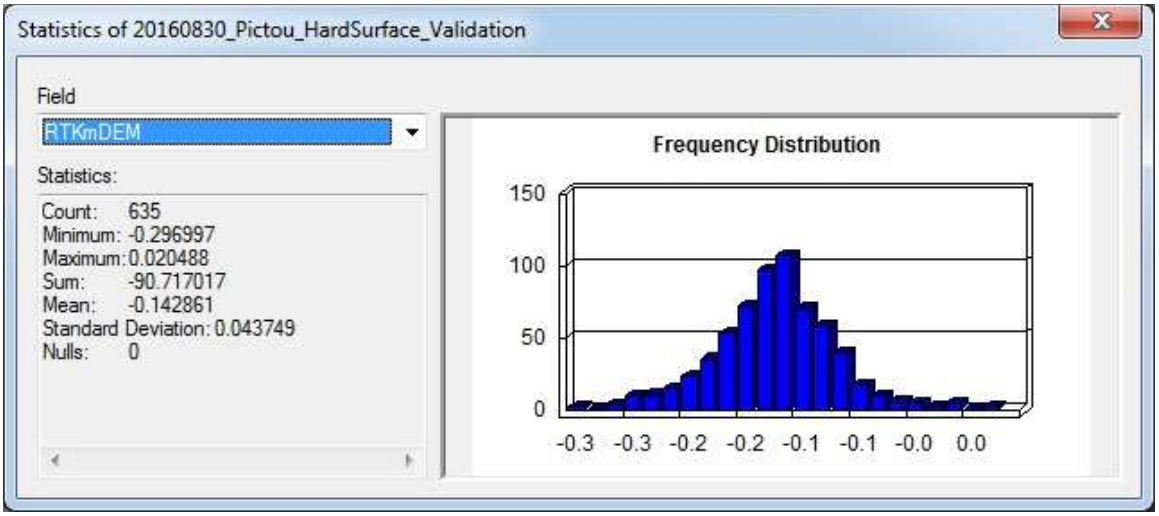

Figure 3.1: Topographic lidar validation for Boat Harbour.

3.1.2 Bathymetric Validation

Mean ΔZ was negative, indicating that the DEM elevation is less (shallower) than the observed GPS point. There were 28 points (direct seabed elevation measurements) with mean ΔZ -0.17 m ± 0.25 m (Figure 3-2).

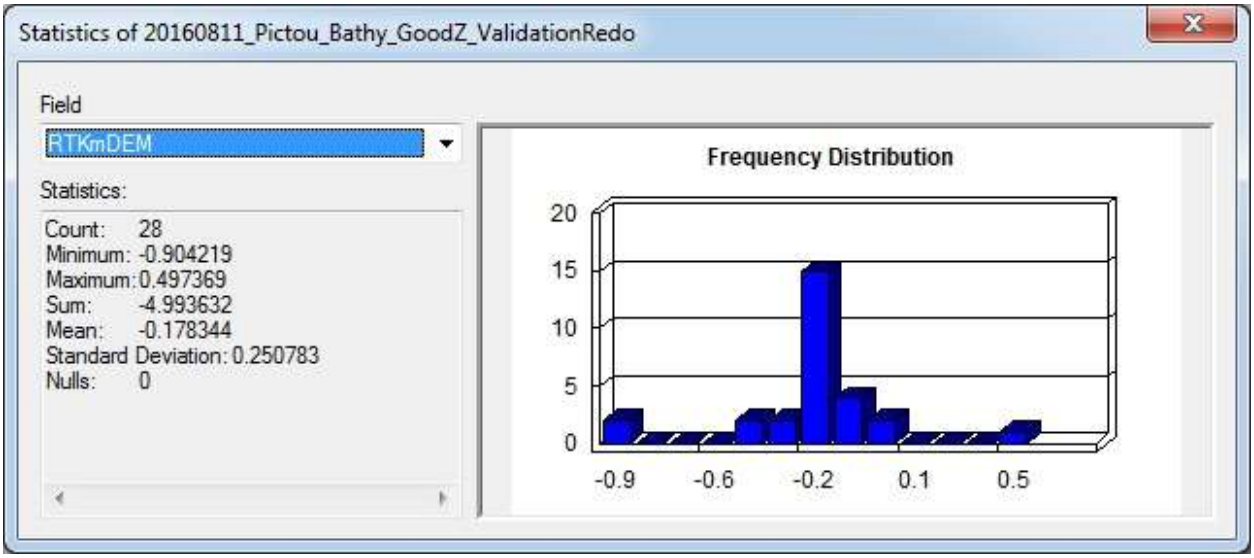

Figure 3.2: Bathymetric lidar validation for Boat Harbour.

3.1.3 Comparison between Multibeam and Lidar

AGRG acquired CHS 5 m multibeam data for Boat Harbour, which provided depth values for the channel and surrounding study area where the lidar sensor did not penetrate. There were areas of overlap between the multibeam data and the lidar, making it possible to compare the data (Figure 3-1) The multibeam data represented depth relative to chart datum, (lowest astronomical tide) however, these data needed to be converted to mean sea level (CGVD28) in order to accurately compare the values to the lidar, which is relative to CGVD28.

To convert the multibeam data to the correct datum, 0.92 m was subtracted from the data using a raster calculator in ArcGIS™ . 0.92 m is the difference between chart datum and mean sea level. With both data sets now relative to the same datum, the data were compared in ArcMap. Raster Calculator was used again to subtract the 'known' data (multibeam) from the lidar. The resulting data was a raster highlighting the areas of overlap between data sets as well as the difference. This dataset was then converted to points in order to interpret the summary statistics for further comparison (Figure 3-2).

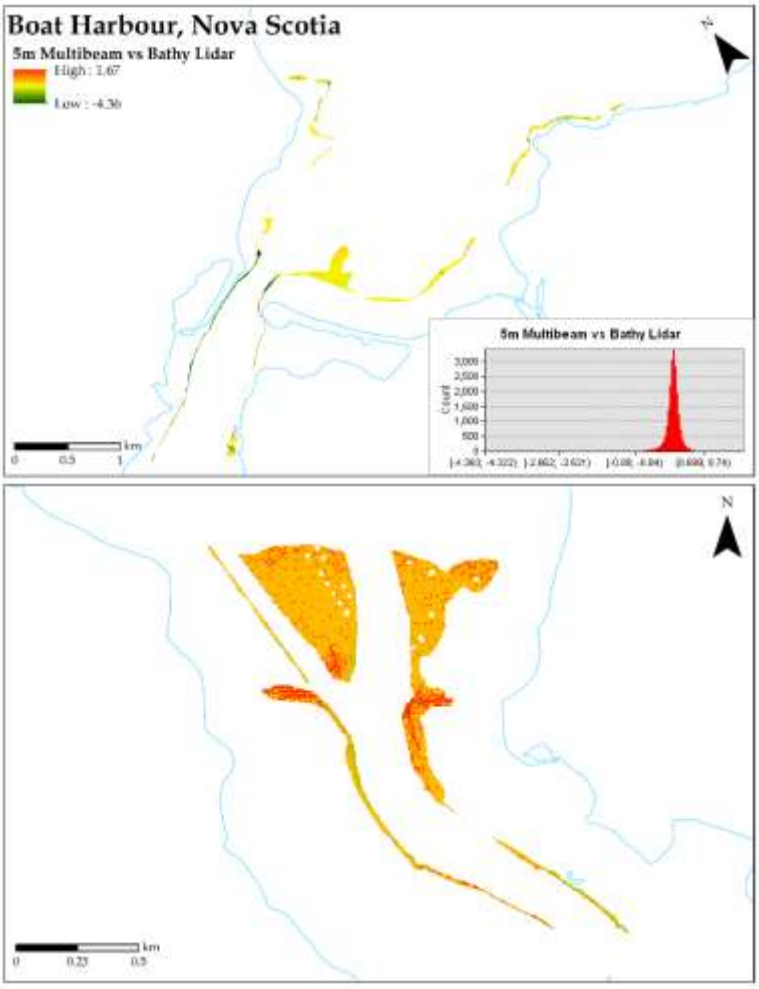

Figure 3-1: Map comparing the CHS 5m multibeam data in Boat Harbour to the lidar acquired by AGRG. The top panel shows the Northern section of study area (data frame rotated 36° to the north), the bottom panel shows the Southern section of the study area. Histogram illustrates a calculated mean ΔZ of -0.03 m ± 0.3 m.

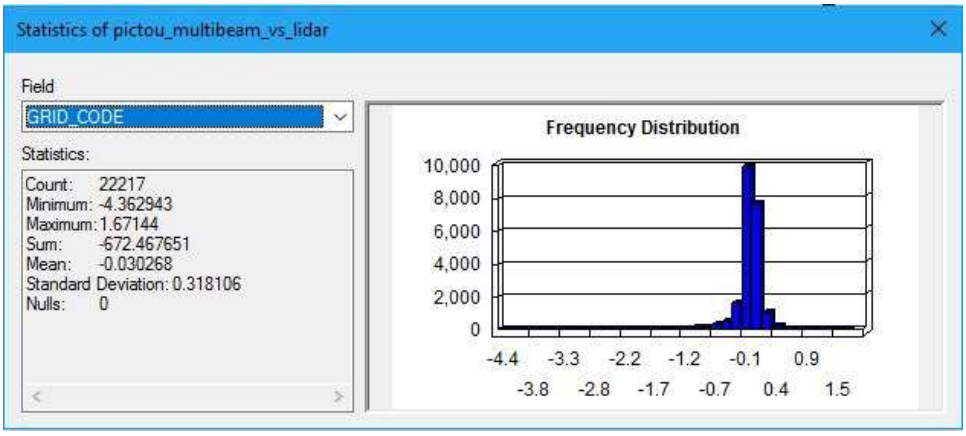

Figure 3-2: Histogram of resulting difference between multibeam and lidar shows a calculated mean ΔZ of -0.03 m ± 0.3 m.

3.2 Surface Models and Air Photos

3.2.1 Digital Elevation Model

Lidar penetration at Pictou Harbour was successful in the nearshore areas of the study area, penetrating to a maximum of -4.8 m CGVD28 (which roughly corresponds to an equivalent depth), located near the northwestern portion of Pictou Harbour (Figure 3-3). The lidar revealed sandbars, channels amidst flat, shallow coves, and complex nearshore topography. In the southern study area, near the submerged pipe, the lidar penetrated to -3 m CGVD28 (Figure 3-4). The lidar did not penetrate an area approximately 1 km long, and 400 m at its widest area, located at the mouth of Boat Harbour (Figure 3-3 shown as missing data, Figure 3-5). Poor water clarity resulted in the bathymetric laser reflecting off the surface of the water and not penetrating through the cloudy water.

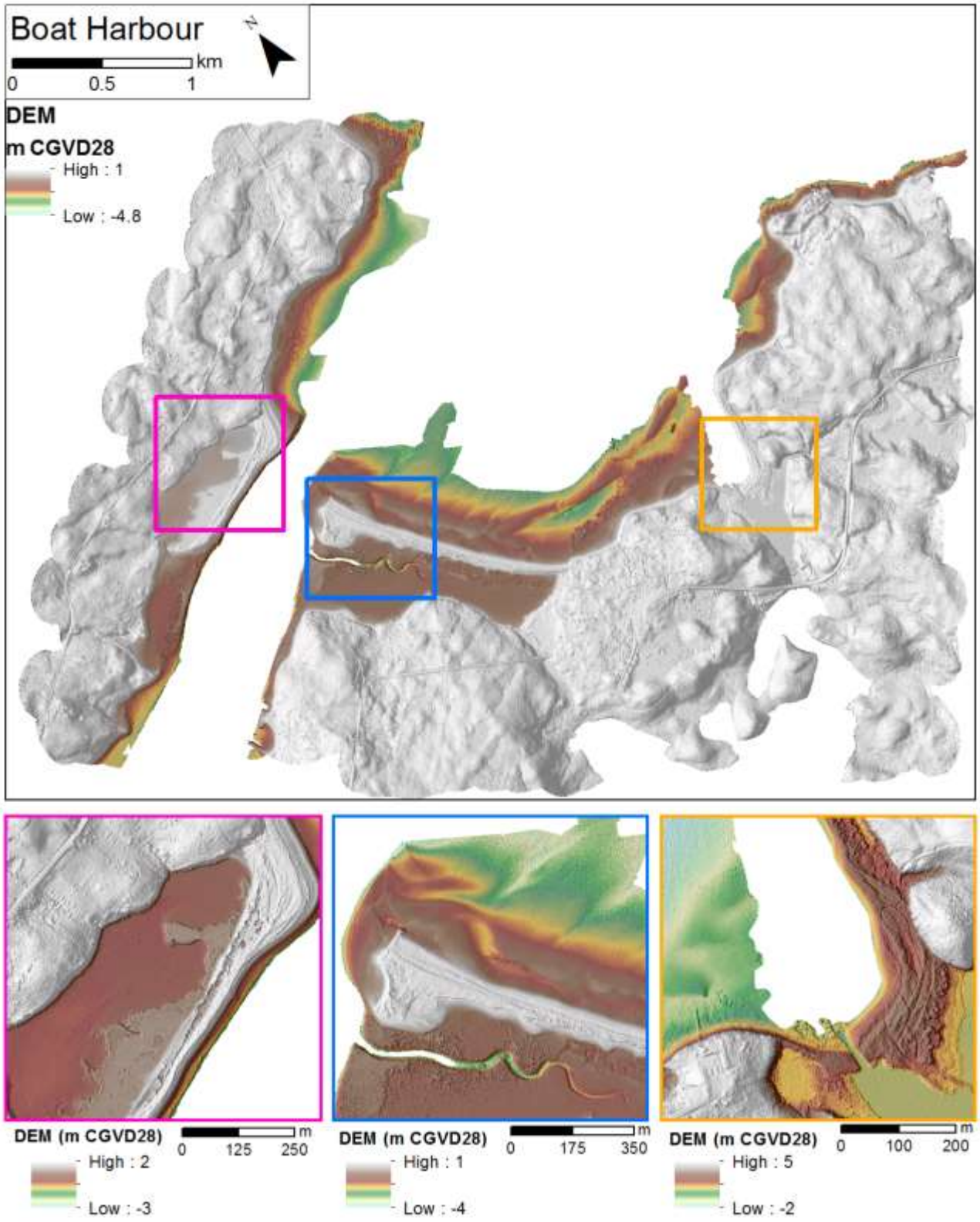

Figure 3-3: Digital Elevation Model for Boat Harbour, draped on a 5x hillshade, scaled to show bathymetry relief for the Northern section of study area (rotated 36° to the north), and with insets showing smaller features. Insets are matched to the larger figure by border colour.

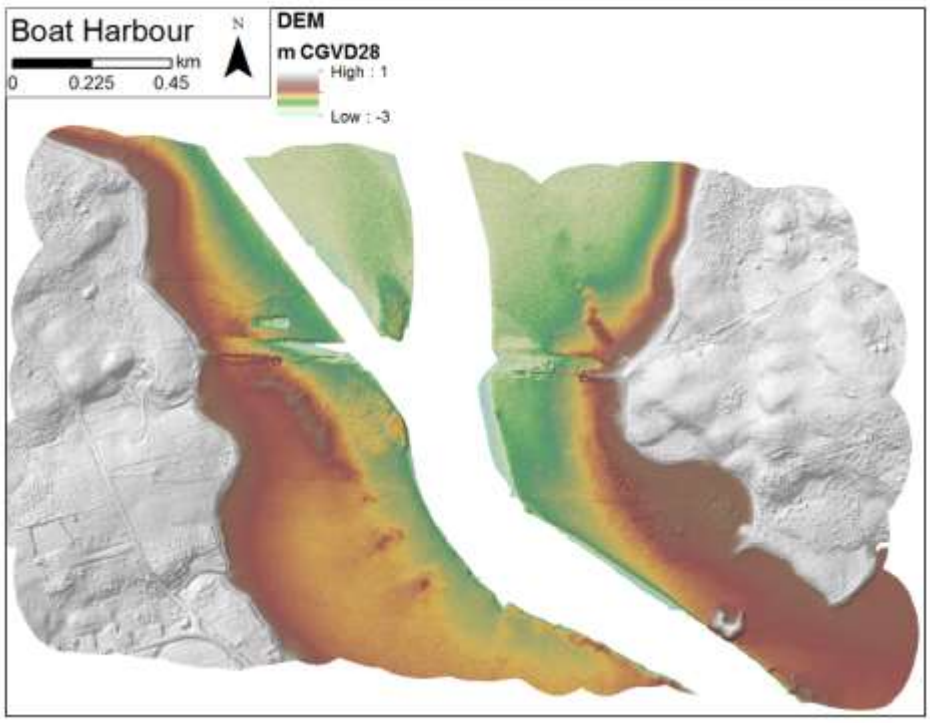

Figure 3-4: Digital Elevation Model for Boat Harbour draped on a 5x hillshade, rotated and scaled to show bathymetry relief for the Southern section of study area.

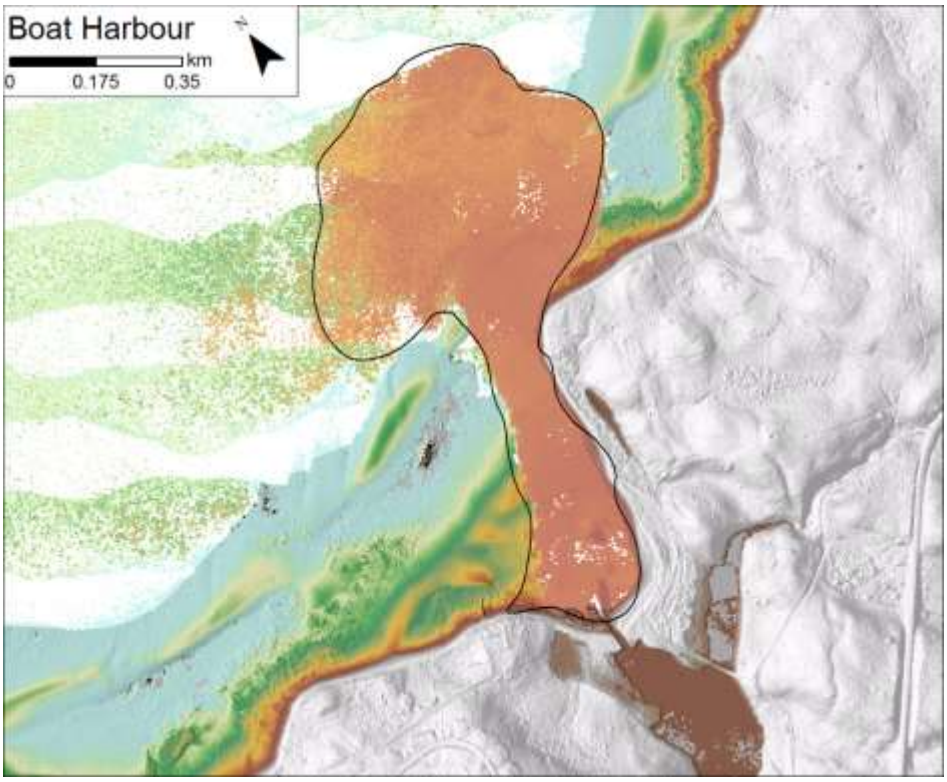

Figure 3-5: The raw (uncleaned) lidar DEM showing how the laser reflected off the opaque plume (outlined) located at the mouth of Boat Harbour.

3.2.2 Colour Shaded Relief Model

The Colour Shaded Relief (CSR) models show the topographic relief in shades of green-red-yellow, and the bathymetry relief in shades of blue where darker blue represents deeper water. CSRs provide an exaggeration of the DEMs and DSM's (5x actual height) and include artificial shading to accentuate topographic and bathymetric features. These maps are especially useful for identifying where the land ends and the water begins; for example, in Figure 3-6 the pink panel clearly identifies the nearshore area.

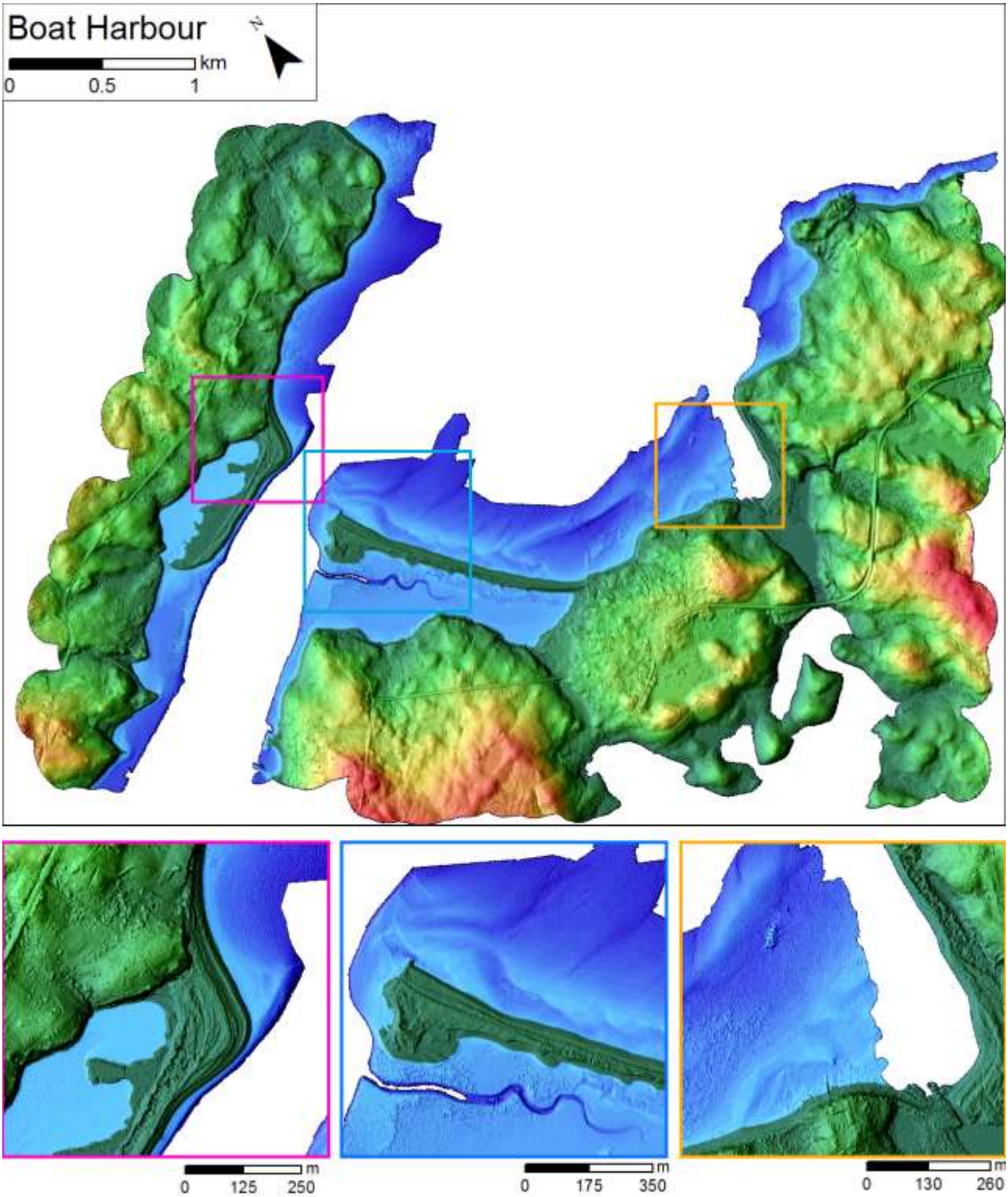

Figure 3-6: Colour Shaded Relief for Boat Harbour, scaled to show bathymetry relief for the Northern section of study area (rotated 36 ° to the north), and with insets showing smaller features. Insets are matched to the larger figure by border colour.

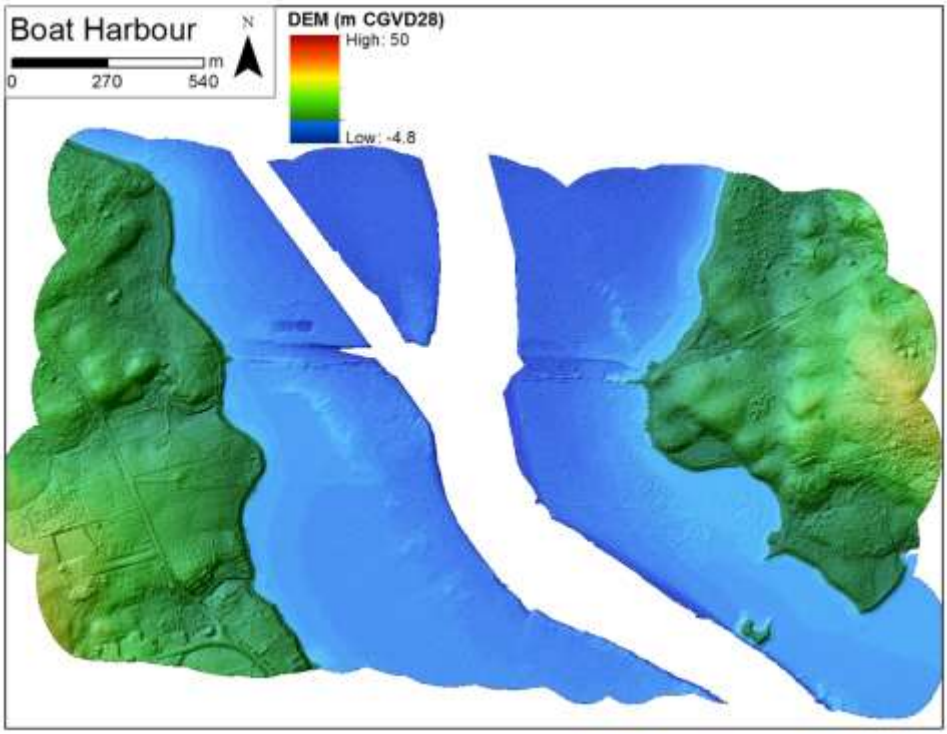

Figure 3-7: Colour Shaded Relief for Boat Harbour, scaled to show bathymetry relief for the Southern section of study area.

3.2.3 Depth Normalized Intensity

The Depth Normalized Intensity models (DNIs) can be a powerful tool to reveal submerged features and bottom type information that the air photos and DEM may not depict. The intensity data show the contrast between brightly coloured seabed and the dark colour of eelgrass or other submerged vegetation. The DNI maps suggests the presence of vegetation in the shallowest areas and south of the harbour mouth, and suggests that the seabed is mainly composed of sand north of the harbour mouth, with bands of darker vegetation in the nearshore (Figure 3-8, Figure 3-9).

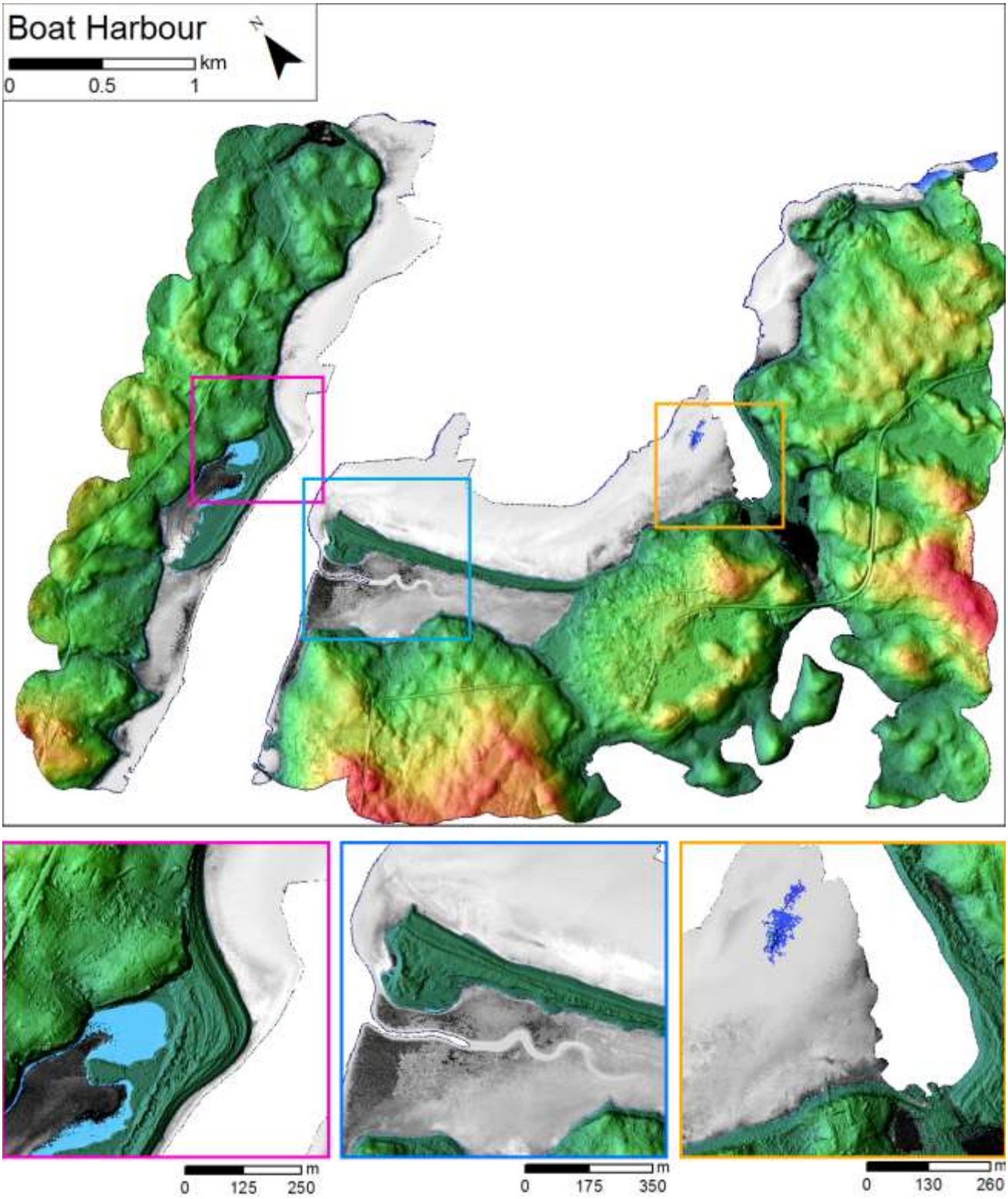

Figure 3-8: Depth-normalized intensity model (for bathymetry only) draped over the CSR, rotated 36° to the north. Typically, darker areas represent submerged vegetation, while brighter areas represent sand. Insets are matched to the larger figure by border colour.

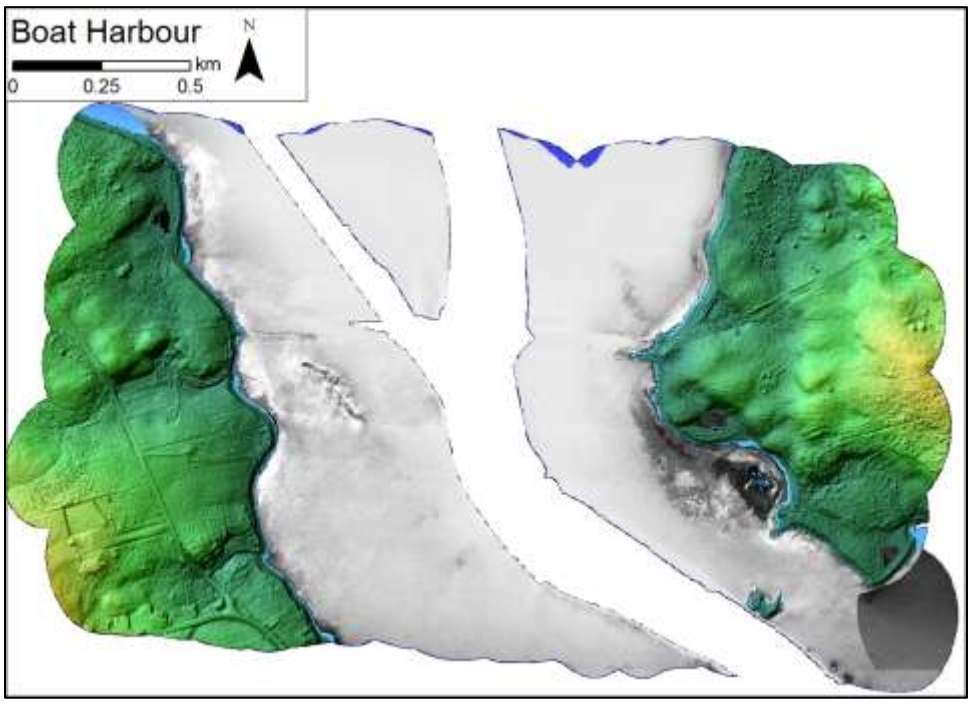

Figure 3-9: Depth-normalized intensity model (for bathymetry only) draped over the CSR. Typically, darker areas represent submerged vegetation, while brighter areas represent sand.

3.2.4 Air Photos

The aerial orthophoto mosaics provide insight into land use, water clarity, bottom type, wave action, and river morphology. The orthophoto panels show the different levels of water clarity throughout the study area (Figure 3-10, Figure 3-11). At Boat Harbour, submerged features such as sediment and sand ripples can be seen in both the blue and orange panels; additionally, a deep channel is visible in the blue panel.

Figure 3-10: Orthophoto Mosasic for Boat Harbour (rotated 36° to the north), and with insets showing smaller features. Insets are matched to the larger figure by border colour.

Figure 3-11: Orthophoto Mosaic for Boat Harbour, scaled to show bathymetry relief for the Southern section of study area.

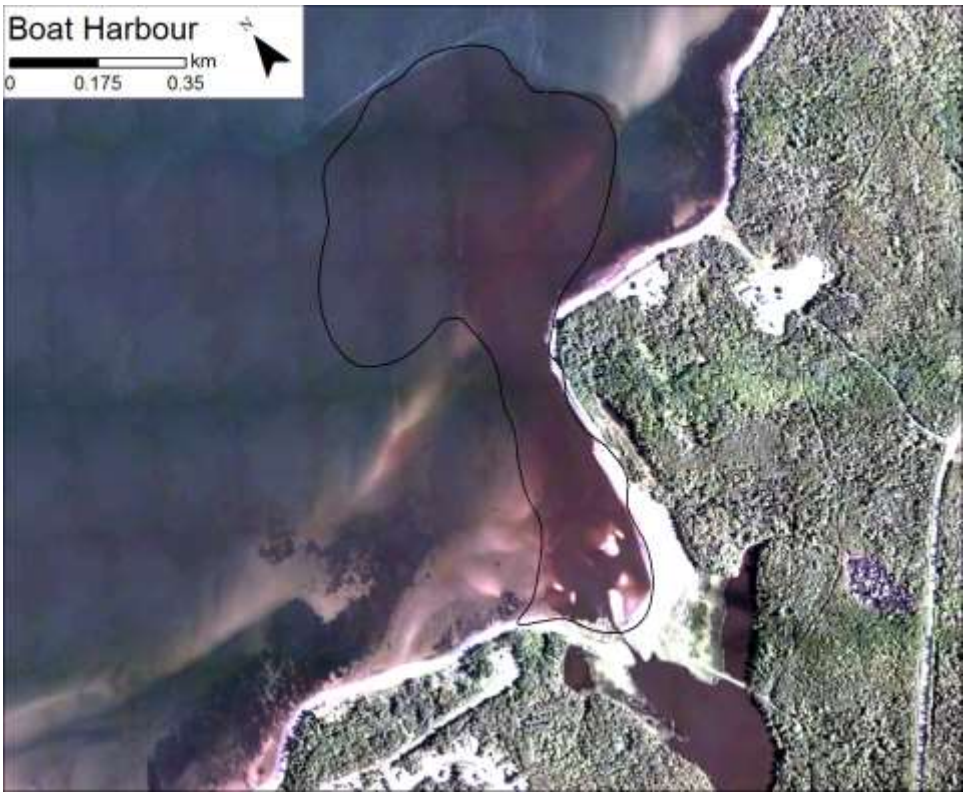

Figure 3-12: Orthophoto mosaic showing the plume of dark water near the mouth of Boat Harbour, outlined in black.

3.3 Ground Truth Maps

The underwater photographs taken using a GoPro camera mounted to a quadrat are useful indicators of bottom type throughout the study area. The following sections present some of the images obtained during the field season displayed on the RCD30 5 cm resolution orthophoto mosaics.

3.3.1 Boat Harbour

The bottom type at Boat Harbour was a combination of sand, mud, fucus and eelgrass. The water appears mainly clear in the inner bay, North West of Pictou (Figures 3.9 – 3.12). Towards Pictou Landing, on the Eastern side of the study area, the water is darker and the bottom appears to be composed mainly of mud and sand with a small amount of fucus present. (Figure 3.12)

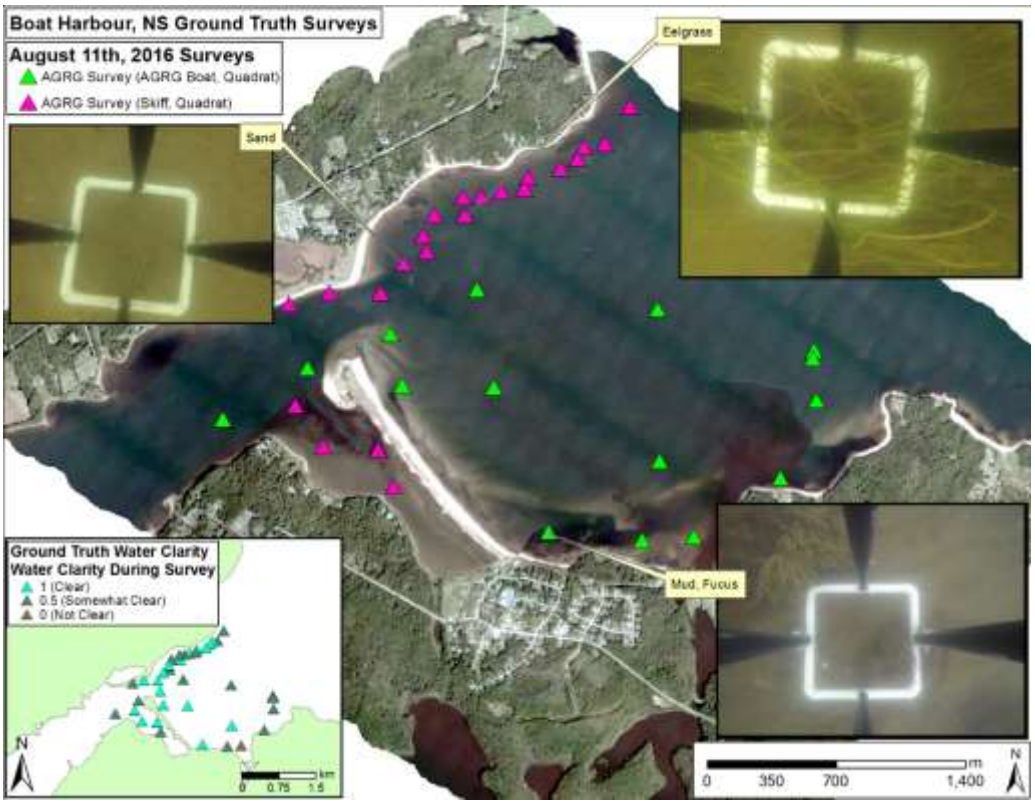

Figure 3-13: Boat Harbour underwater photo ground truth for both surveys (AGRG and partner boats). Background image is RCD30 orthophoto RGB mosaic.

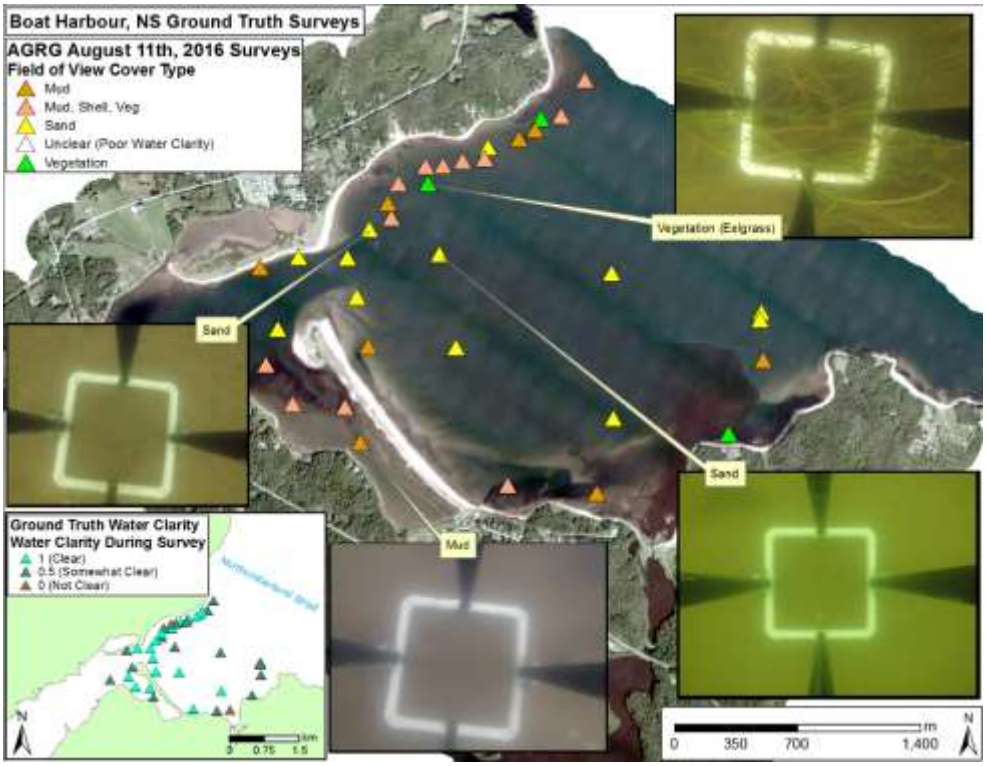

Figure 3-14: Boat Harbour underwater photo ground truth for both surveys (AGRG and partner boats) symbolized to show the field of view cover type. Background image is RCD30 orthophoto RGB mosaic.

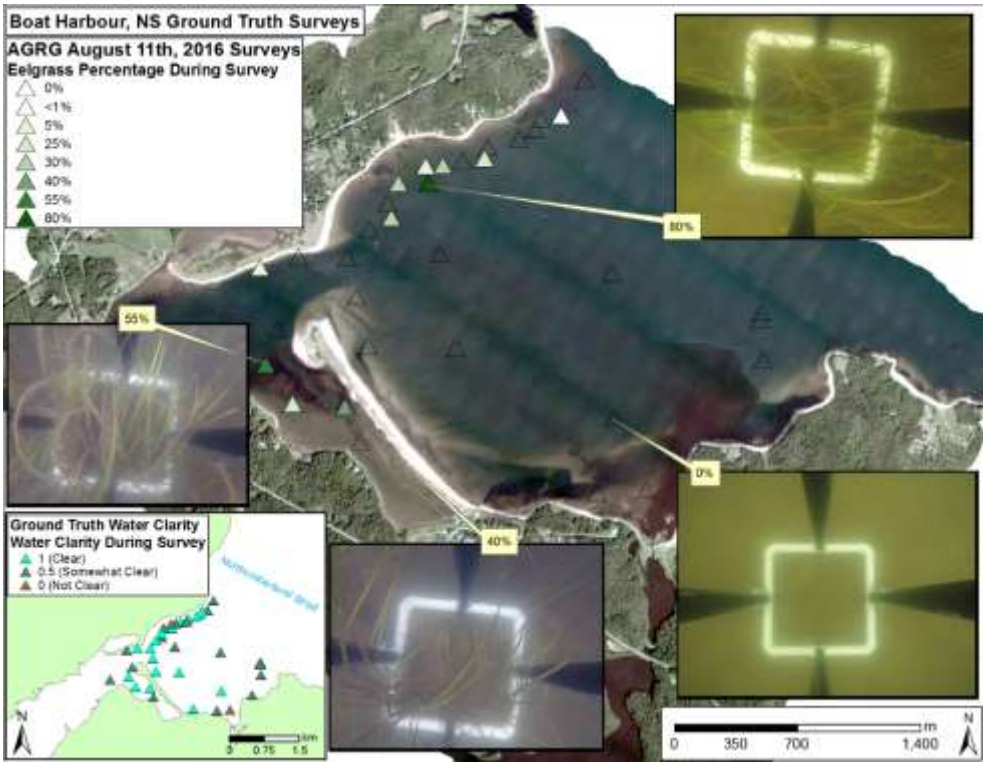

Figure 3-15: Boat Harbour underwater photo ground truth for both surveys (AGRG and partner boats) symbolized to show the eelgrass percentage. Background image is RCD30 orthphoto RGB mosaic.

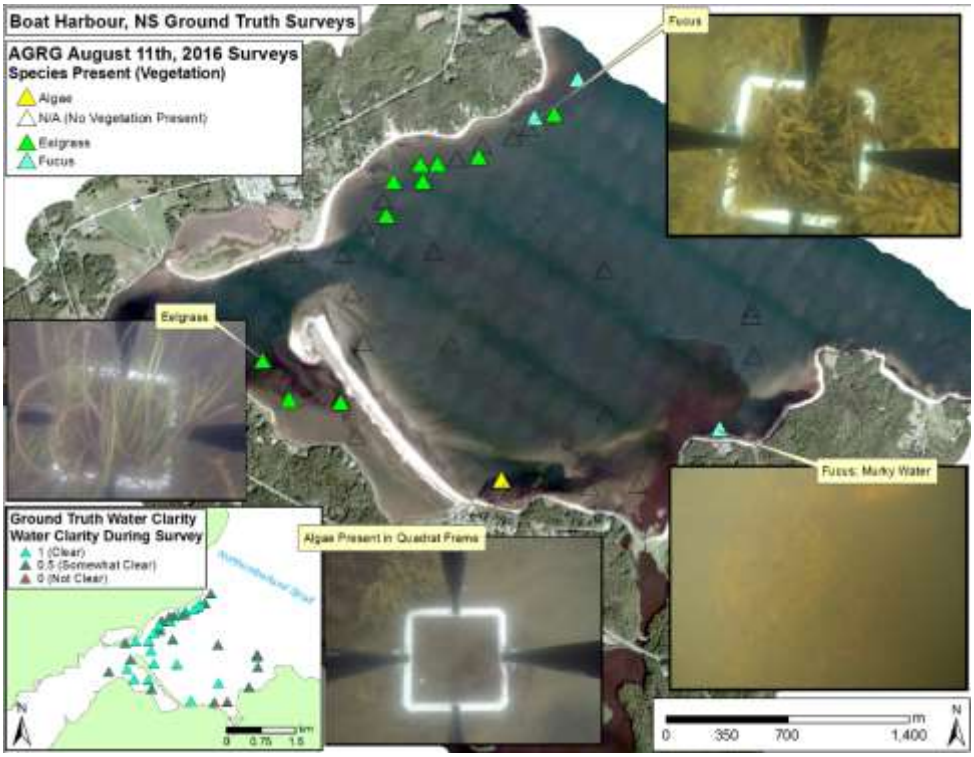

Figure 3-16: Boat Harbour underwater photo ground truth for both surveys (AGRG and partner boats) symbolized to show the species type of vegetation present. Background image is RCD30 orthophoto RGB mosaic.

3.4 Bottom Type Maps

Figures 3-17 to 3-21 depict the bottom type classification and eelgrass distribution produced by the methodology described in section 2.7. Both ground based and boat based ground truth points were compared to the bottom type classification produced and the overall agreement of the classification of eelgrass was 87.5% (Table 4).

Class	Number of Ground Truth Points	Points in Agreement with Classification	Percent Agreement (%)
Eelgrass	8	7	87.5
Fucus	4	4	100
Mud	8	2	25
Sand	3	3	100

Table 4 – Percent agreement between bottom type classification and ground truth points.

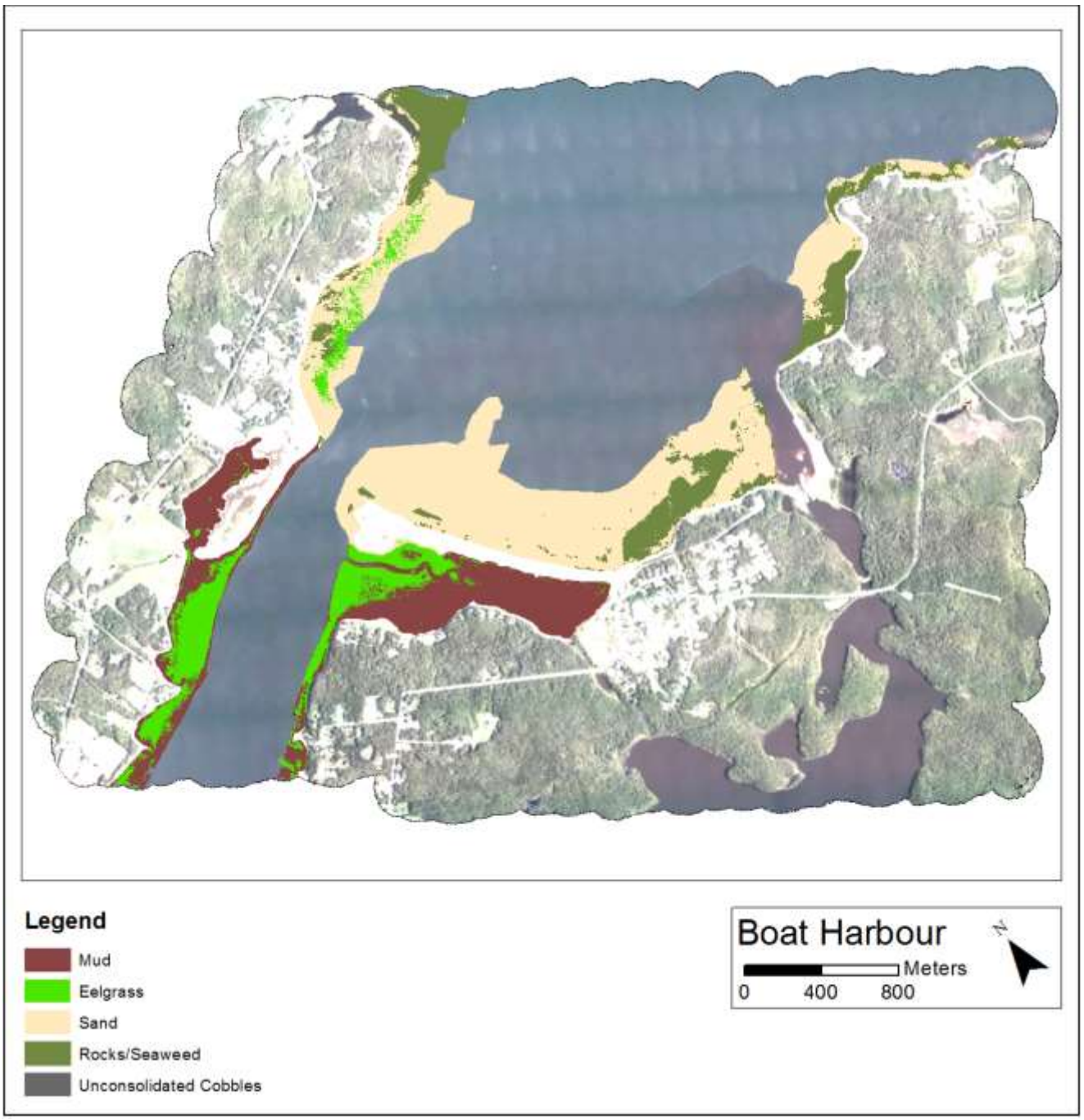

Figure 3-17 – Bottom type classification for Boat Harbour (rotated 36° to the north).

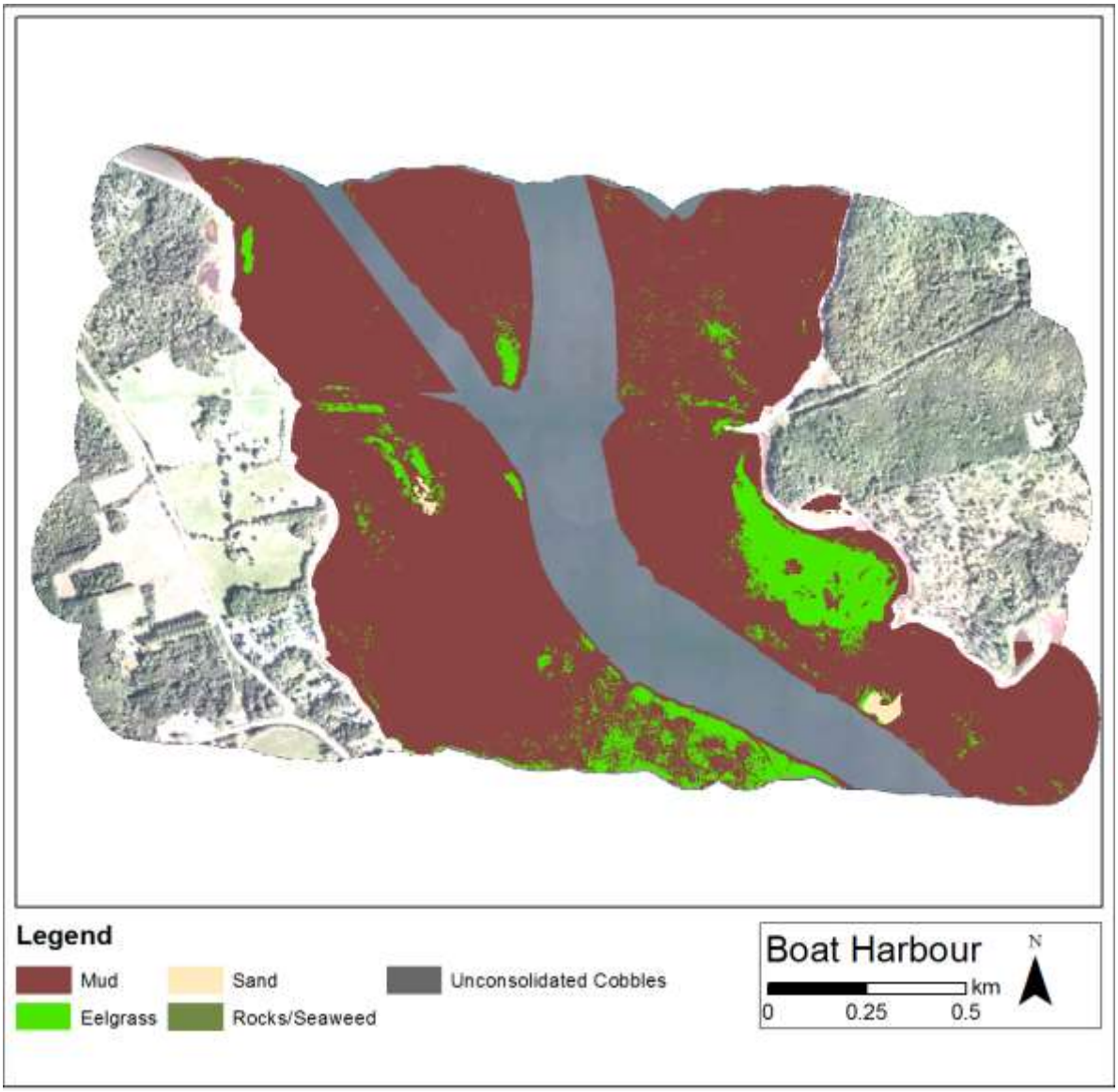

Figure 3-18 – Bottom type classification for the southern portion of the Boat Harbour study area.

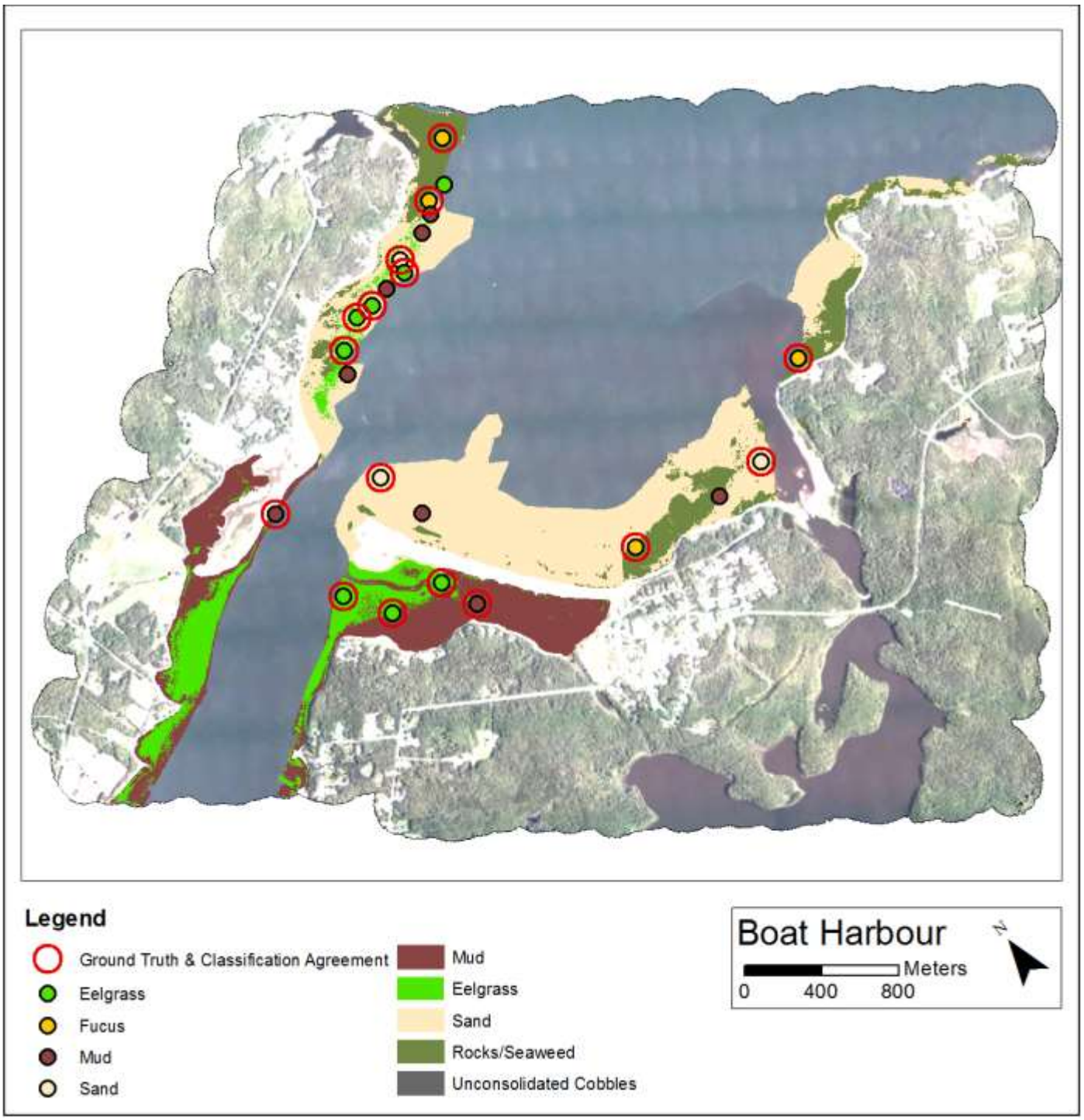

Figure 3-19 – Ground truth and classification agreement based on a sample size of 23 ground truth points. Red circles indicate agreement between the produced classification and ground truth points collected.

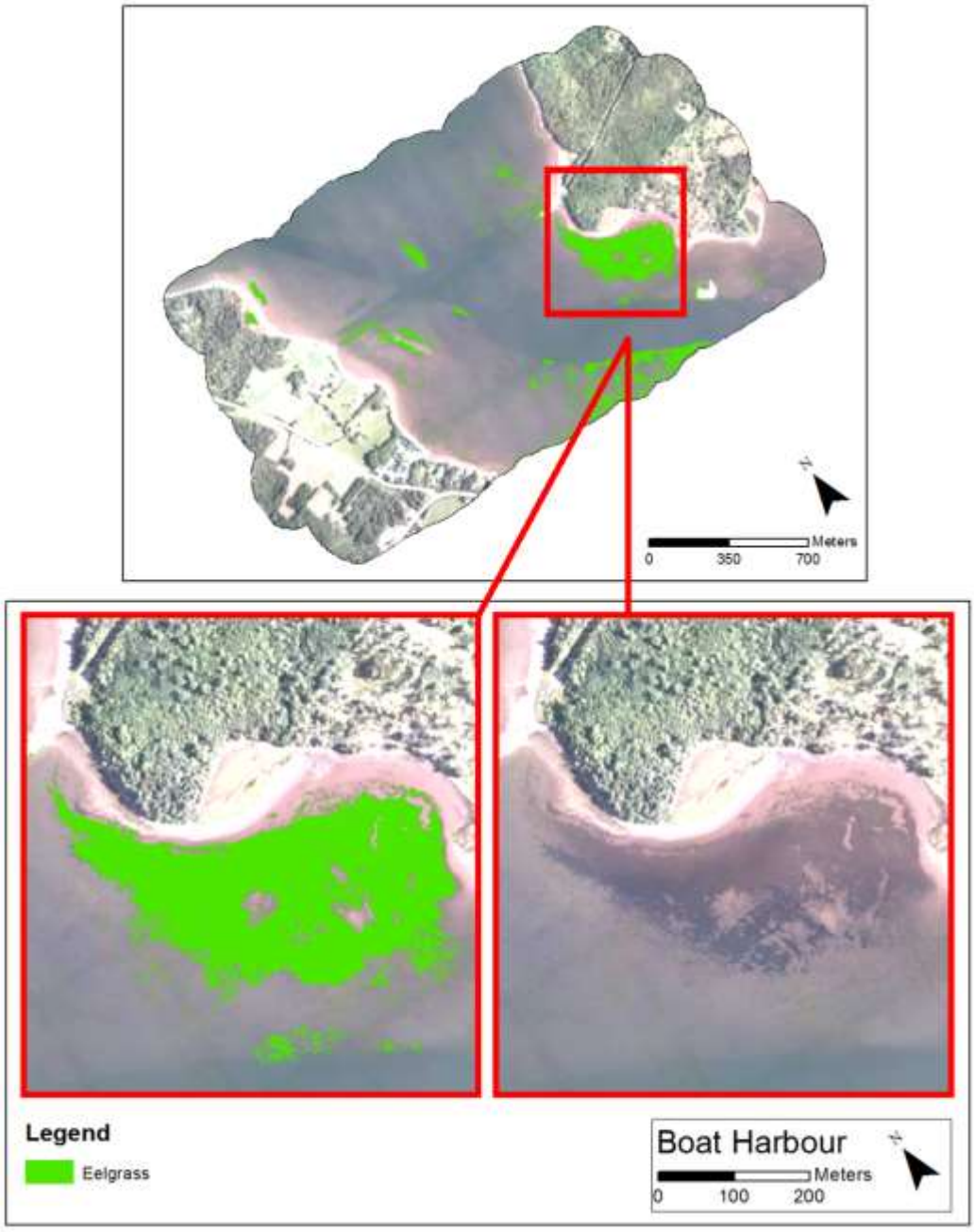

Figure 3-20 – Comparison of bottom type classification of eelgrass to the aerial photograph for the southern portion of the Boat Harbour study area.

Although no ground truth points were collected in the southern portion of the study area, eelgrass is visible on the aerial photograph and appears to be in very good agreement (Figure 31).

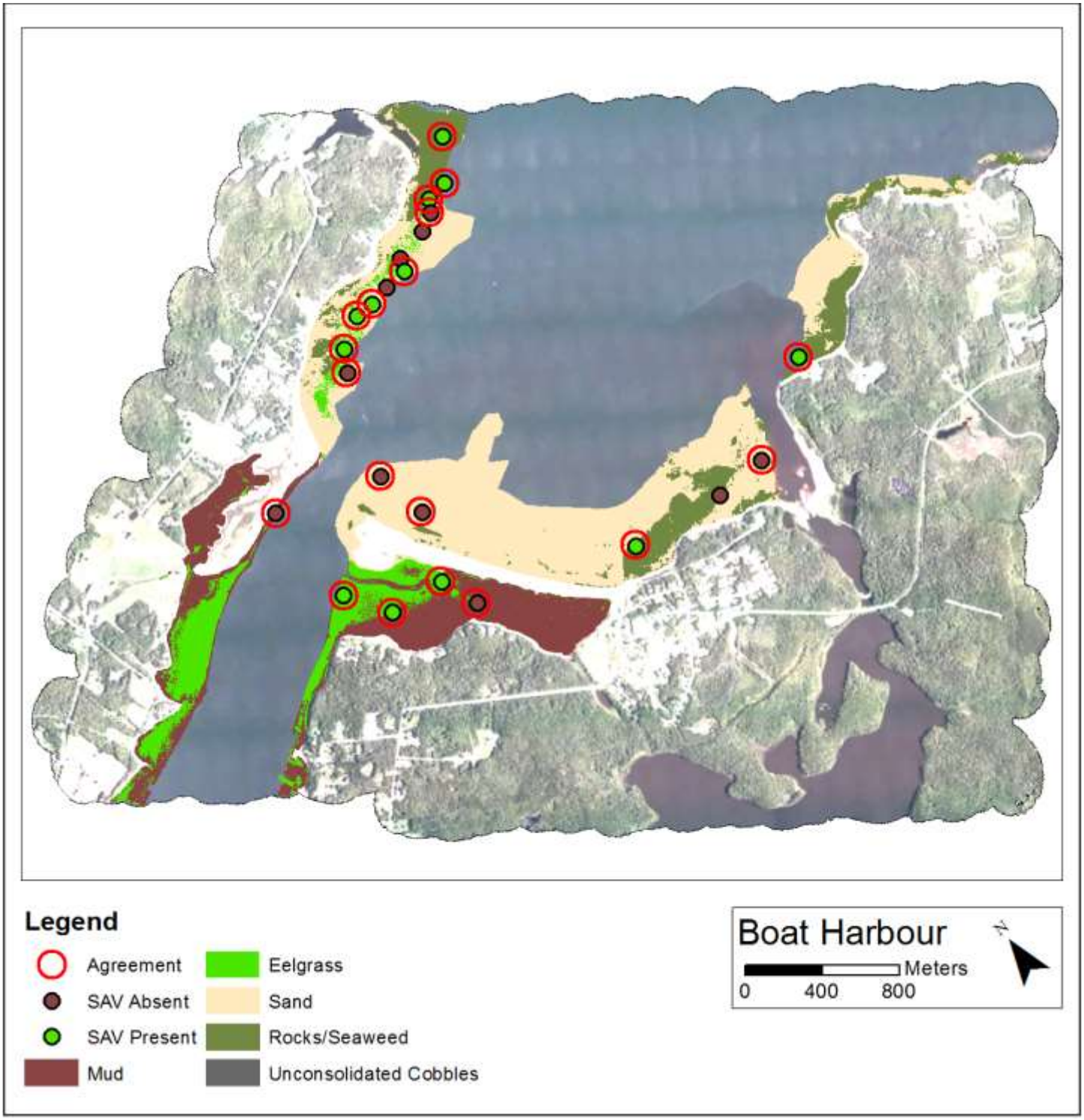

Figure 3-21 – Submerged aquatic vegetation (SAV) presence and absence. The red circles represent ground truth points which agree with the classification.

Figure 3-21 depicts the agreement between the presence and absence between the classification and ground truth data collected. The classification and ground truth points collected agreed very well with each other.

4 Hydrodynamic Model

A high-resolution 2-D hydrodynamic (HD) model was developed using the DHI Mike-21™ software module to simulate current flow and water level variations within the Pictou Harbour study area. The model domain was designed to be much larger than the lidar study area in order to properly model the circulation in the region through the Northumberland Strait into Pictou Harbour. Model inputs included bathymetry and boundaries, described in the following sections.

4.1 Modelling Methods

4.1.1 Grid Preparation

A variety of sources and resolutions of topography and bathymetry were required in order to complete the model depth grid (Table 5, Figure 4-1). Topo-bathymetric lidar data from 2014 (Little Harbour) and 2016 (Merigomish Harbour and Pictou Harbour) were down-sampled from 1 m to 9 m for computational efficiency. Other bathymetric data included a digital compilation of bathymetry data from various sources (e.g. multibeam, single beam, seismic, etc.) aggregated by CHS (Varma et al., 2008) between 5 and 20 m resolution, and 5 m multibeam data for Pictou Harbour and approach. A 20 m resolution database from the Nova Scotia Dept. of Natural Resources was used for the NS topography not included in the lidar dataset, and topographic lidar data collected by AGRG for PEI was used for the PEI coastline.

Provider	Source	Native Resolution	Domain
AGRG	Lidar: Pictou Harbour, Merigomish Harbour, Little Harbour	2 m	Topo/Bathy
CHS	Multibeam: Pictou Harbour and approach	5 m	Bathy
CHS	Chart soundings, echo sounding data, etc.	Variable	Bathy
AGRG	Lidar: PEI	2 m	Topo
NSDNR	Rasterized 1:10 000 Contour Data	20 m	Topo

Table 5: HD model bathymetric data sources, resolution, domain and number of observations. NSDNR: Nova Scotia Department of Natural Resources.

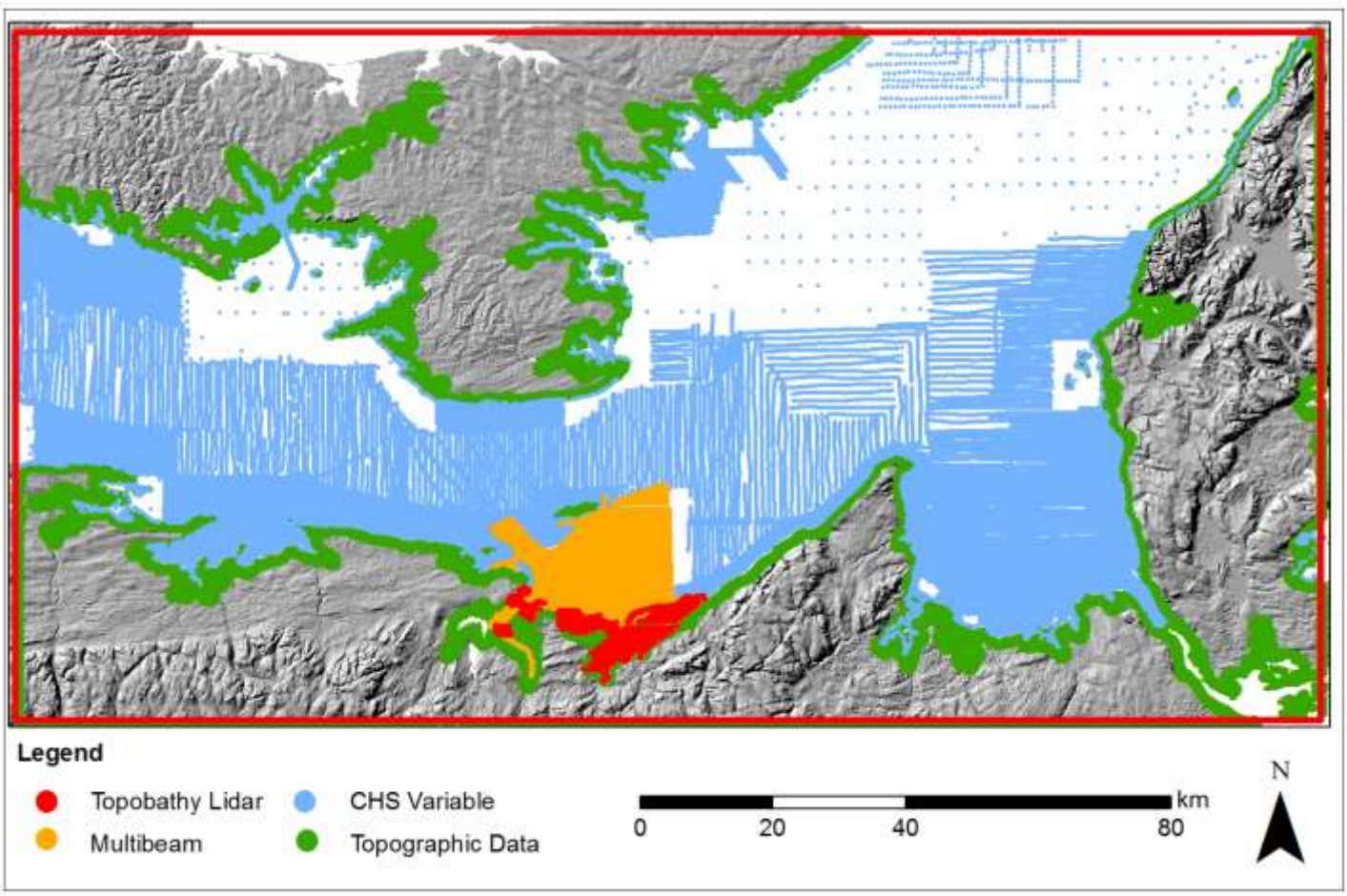

Figure 4-1: Sources of model topographic and bathymetric data.

A nested grid model approach was used to reduce the calculations required by the model. Five different model domains were developed using a 3:1 resolution step (Table 6, Figure 4-2). To generate the grids, the bathymetric and topographic datasets were subject to rigorous quality control procedures to ensure continuity between the various data sources. These datasets were then clipped to remove overlapping data points, giving preference to the higher resolution dataset, and topographic datasets were clipped to the coastline to reduce dataset size. The lowest resolution grids (Domains 4 and 5) were generated using only the coastal topographic data points and the CHS database bathymetry points, and were interpolated into rasters at their required resolutions (243 m and 729 m) using the ArcMap *Topo to Raster* tool to fill gaps in the different resolution datasets. The interpolation technique ensured a smooth elevation surface despite the coarse and irregular point spacing of the different datasets. All of the datasets (lidar, multibeam, topo points, etc.) were used to generate a 9 m resolution dataset to fit Domain 3; this was resampled and clipped to make the remaining model domains (Figure 4-3).

Domain	Resolution (m)
1	9
2	27
3	81
4	243
5	729

Table 6: Nested model domains as shown in Figure 4-2.

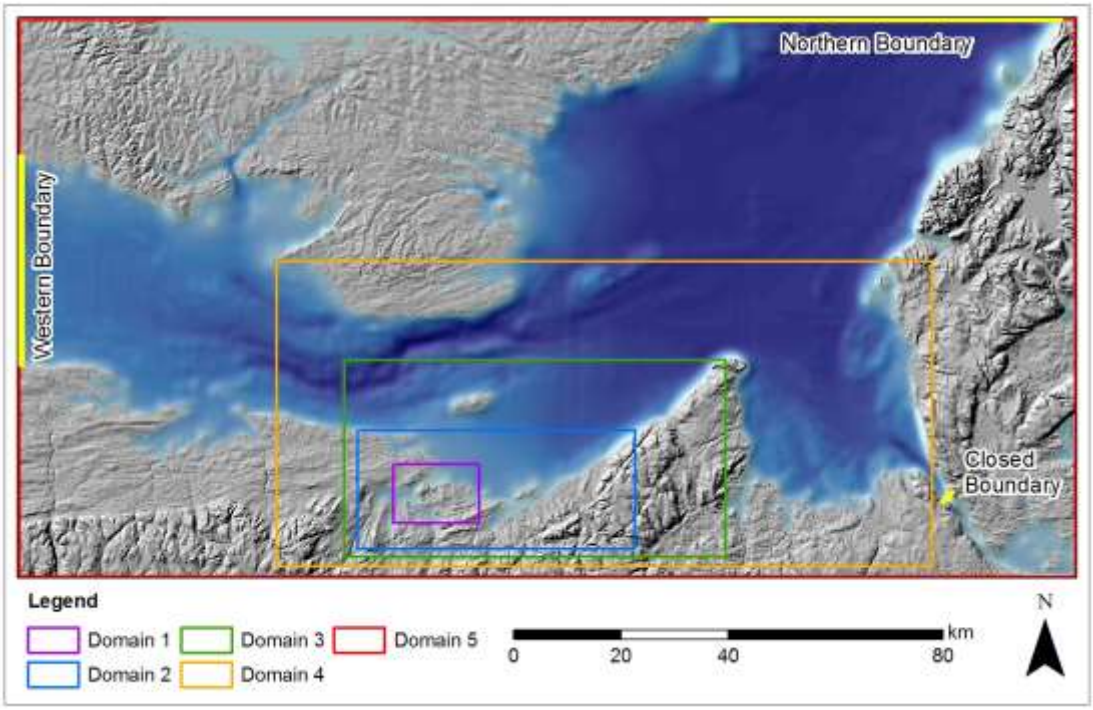

Figure 4-2: Mike 21 hydrodynamic model domain extents, boundaries, and Domain 5 grid draped over a 5x hillshade.

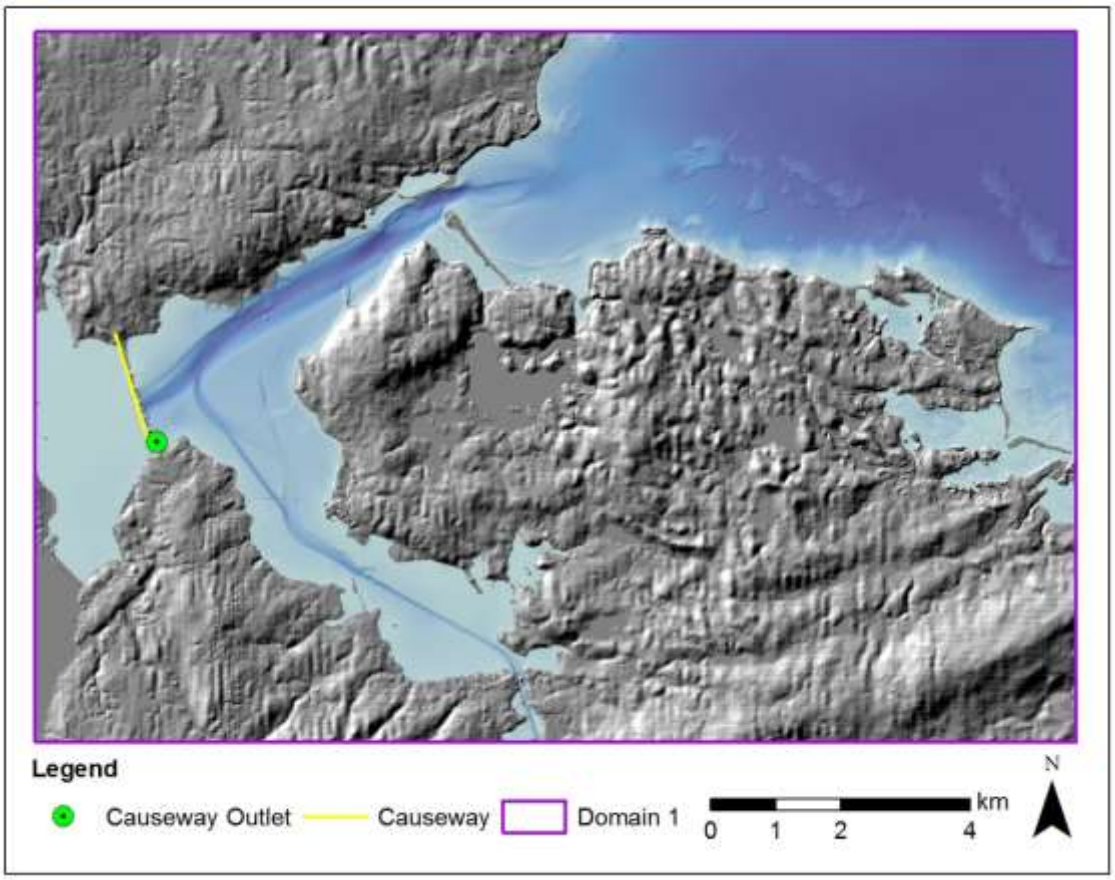

Figure 4-3: Domain 1: 9 m model grid draped over a 5x hillshade; Domain 2: 27 m model grid draped over a 5x hillshade. The Pictou Causeway is represented as a closed boundary with a point source discharge shown on the map by a green symbol.

4.1.2 Boundaries

The model simulated water level variations over the interpolated bathymetric surface in response to a forcing tidal boundary condition at two different locations. The Western Boundary extended from near Pugwash to PEI, and the Northern Boundary extended from Cape Breton to PEI (Figure 4-2). Both boundaries were forced with predicted tidal elevations at 5-minute resolution extracted from WebTide (Dupont et al., 2005). Tidal elevations across the Western Boundary varied between 0.01 m and 0.05 m and at the Northern boundary elevations across the boundary varied by as much as 0.15 m. The Canso Causeway represented a closed boundary; data south of the causeway were not included in the model domain. The Pictou Causeway was also represented by a closed boundary, as no bathymetric data were available to model the circulation in the harbour west of the causeway. Flow into Pictou Harbour through the causeway was represented by a positive discharge source. The values used to model flow under the causeway were somewhat arbitrary (flow = 2.0 m^3/s, velocity = 0.5 m/s). The values were varied during model calibration, but ideally actual measurements of flow and velocity over several tidal cycles would be used to provide more accurate model input.

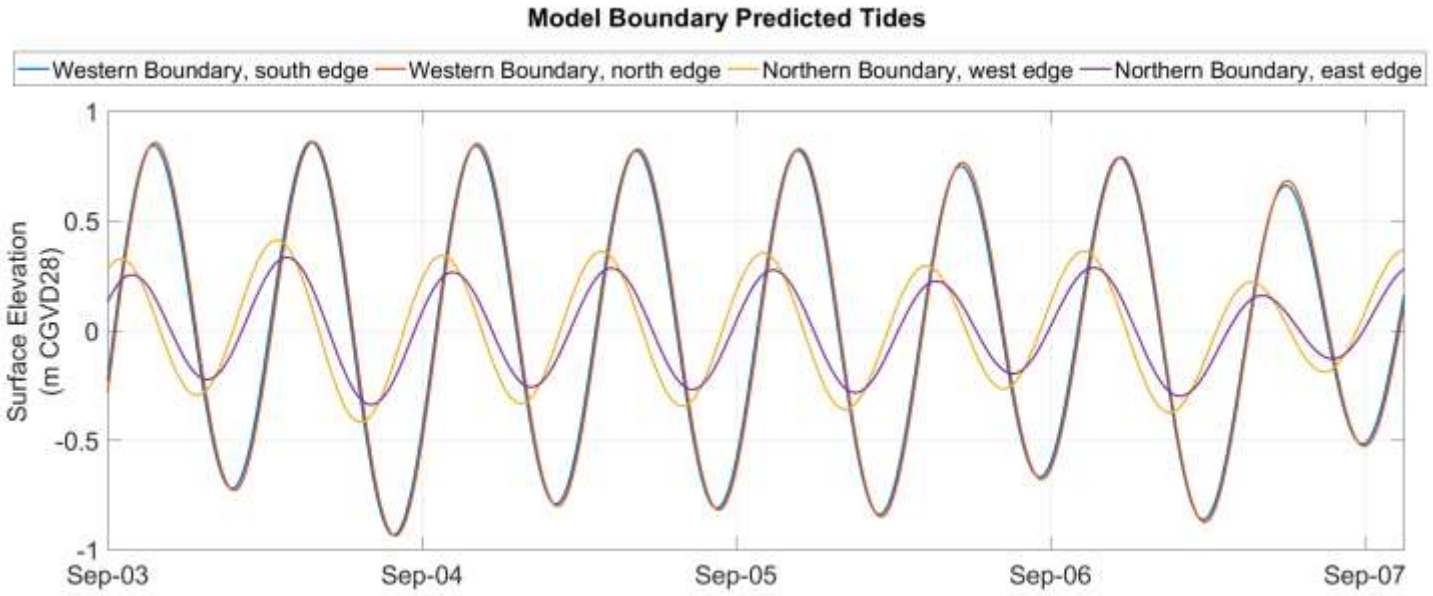

Figure 4-4: Tidal elevations predicted for the duration of the model simulation across the boundaries.

4.1.3 Model Parameters and Calibration

Parameters used in the model simulation are reported in Table 7. The model simulation start time (Sept. 3, 2016, 2:00) was chosen to overlap with observed currents and surface elevation, and to coincide with a high tide, for model stability. The calibration simulation lasted for two days, and model parameters were optimized by comparing model results to observations. The timestep (Δt) was chosen in order to minimize the Courant number, *C*, which was calculated based on

$$C = \sqrt{\mathrm{g} \times z_{max}} \times \frac{\Delta t}{\Delta x}$$

where z_{max} is the maximum depth for each model grid, g is gravity, and Δx is the model resolution. A grid-dependent, velocity-based eddy viscosity scheme produced the best results. A constant eddy viscosity value, *E*, was calculated for each model domain as such

$$E = 0.02\frac{\Delta x^2}{\Delta t}$$

following guidelines in a Mike 21 manual (DHI Water & Environment, 2008). The bed resistance value was varied between a Manning's M of 32 $m^{1/3}/2$ and 48 $m^{1/3}/2$; a value of 44 $m^{1/3}/2$ produced the most stable results. Effects of wind and waves were not modelled at this time.

Domain	Resolution (m) Δx	Courant Number	Eddy Viscosity (m^2/s)	Resistance ($m^{1/3}/2$ Manning's M)	Initial surface elevation (m)	Timestep (s) Δt	Drying Depth (m)	Flooding Depth (m)
1	9	5.70	0.32	44	0.5	4	0.01	0.02
2	27	2.51	2.92					
3	81	1.17	26.2					
4	243	0.43	236					
5	729	0.15	2126					

Table 7: Model Parameters.

4.1.4 Validation

The model was validated by simulating flow between Sept. 3, 2016 at 2:00 and Sept. 7 at 2:00 and comparing results to surface elevation and currents measured by the ADCP, and assessing the two-dimensional circulation of flow throughout Pictou Harbour.

The modelled surface elevation agreed well with the observed surface elevation, and exhibited an R^2 value of 0.92, Pearson coefficient of 0.96, and homogeneous distribution of residuals (Figure 4-5). The modelled east-west currents agreed well with the phase of the observations, but the model did not consistently simulate the observed variation in amplitude between tides (Figure 4-6). This resulted in a moderate error analysis (R^2 =- 0.33, Pearson = 0.57, somewhat homogeneous distribution of residuals). The model captured the large-scale nature of the north-south currents, predicting the amplitude of the flood tide but predicting the phase wrong, and modelling some of the finer signals of the southern ebb tide well in phase but under-predicting amplitude (Figure 4-7). The error analysis reflected these imperfections (R2 = 0.12, Pearson = 0.34). Assessment of current speed and direction show a different perspective on the modelled flow. The model simulates a consistent pattern from tidal cycle to tidal cycle, showing strong eastward current speeds on each ebb tide, followed by slower westward current speeds on the flood tide (Figure 4-8). The observations, in contrast, show a greater deal of variability between tidal cycles, although the general nature of the current speed and direction is represented.

Analysis of the depth-averaged ADCP current compared to the currents measured at all depths reveals that the water column at the site of the ADCP exhibited a great deal of variability, often showing eastward flow at one depth, and simultaneous westward flow at another depth (Figure 4-9). This type of flow structure is difficult to model accurately using a depth-averaged, two-dimensional model; however, Figure 4-9 shows that when the flow was well-mixed, or homogeneous throughout the water column and the depth-averaged flow was similar to the flow at each depth (e.g. Sept. 3, 9 PM– Sept. 4, 11 AM), the model simulated the observations well. When there was greater variability in flow between the surface and the seabed and the depth averaged ADCP was not a good representation of average flow (e.g. Sept. 4, 11 APM– Sept. 5, 11 PM), the model did not simulate that depth-averaged flow well.

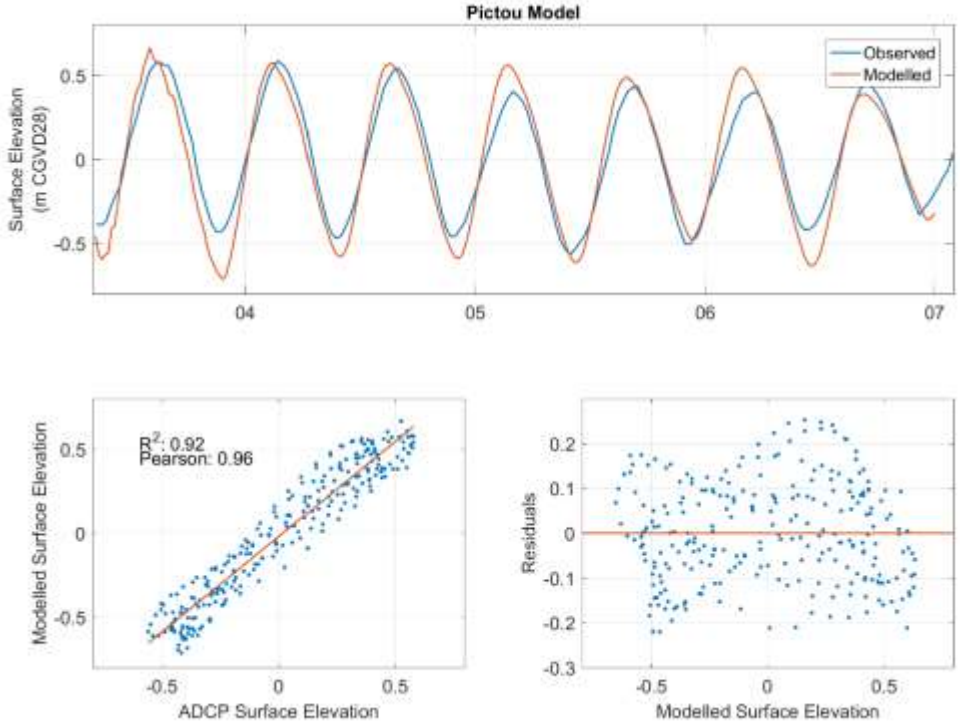

Figure 4-5: Modelled and observed surface elevation (upper panel), and error analysis (lower panels).

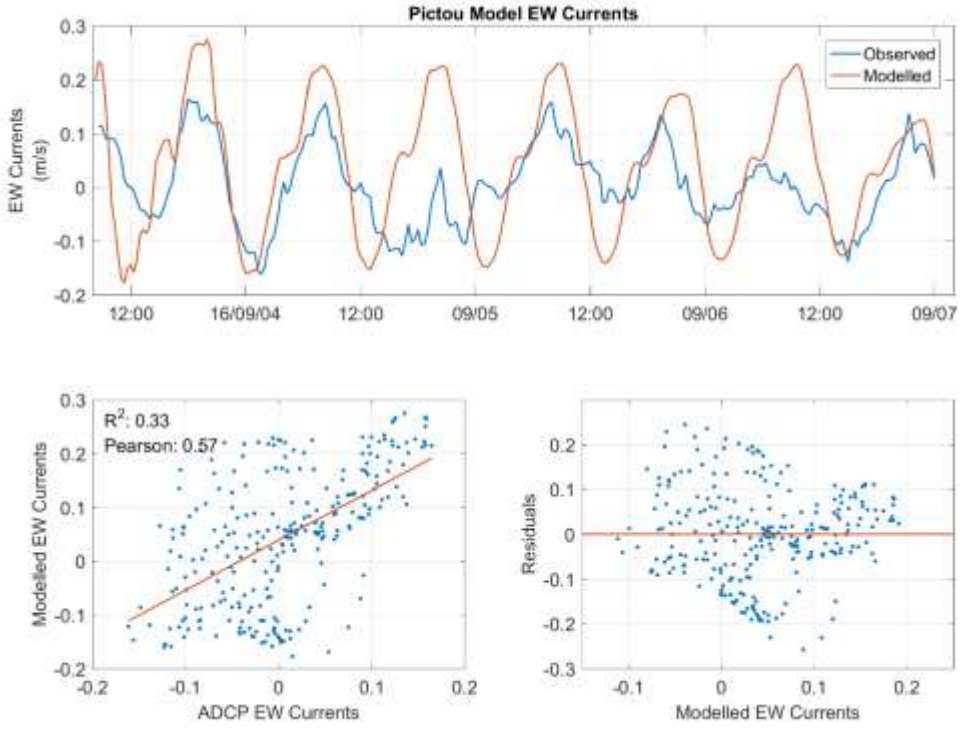

Figure 4-6: Modelled and observed EW current (upper panel), and error analysis (lower panels).

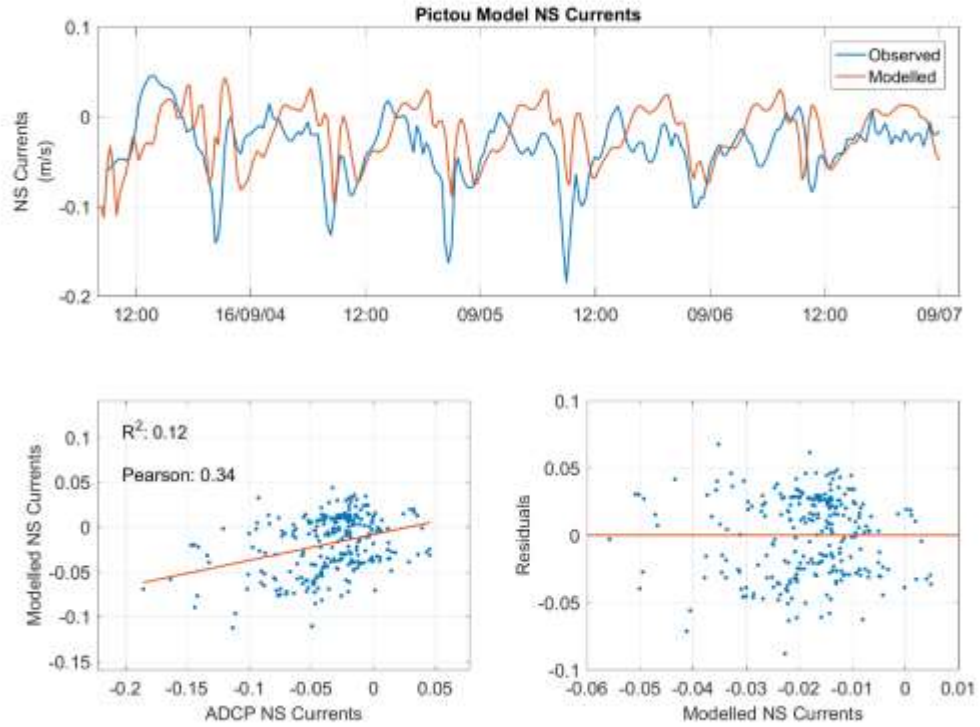

Figure 4-7: Modelled and observed NS current (upper panel), and error analysis (lower panels).

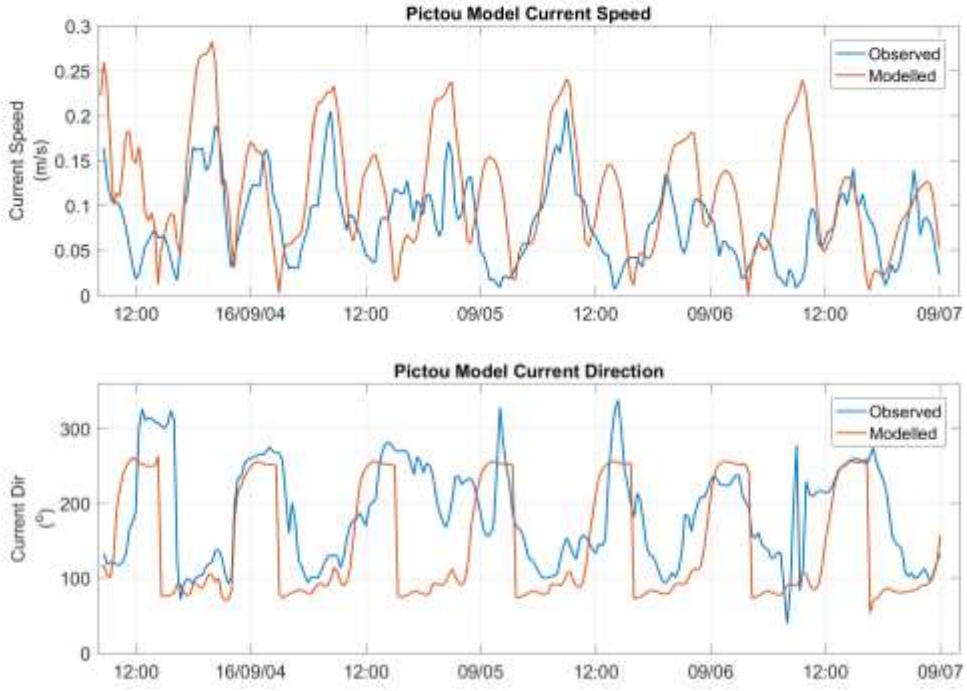

Figure 4-8: Modelled and observed current speed (upper panel) and direction (lower panel).

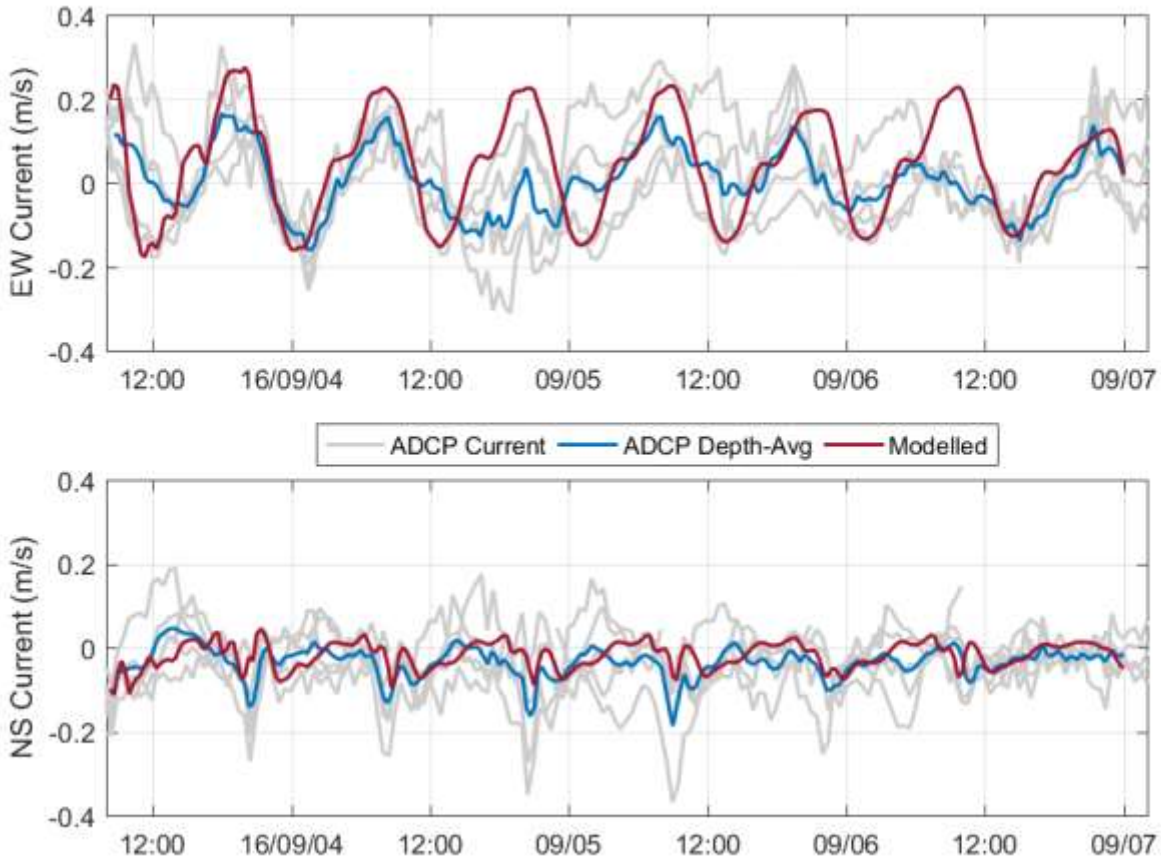

Figure 4-9: Modelled depth averaged current, observed depth averaged current, and currents for each depth as observed by the ADCP. EW currents shown on upper panel, NS currents shown on lower panel.

4.2 Modelling Results

The hydrodynamic model was successful in simulating tidal flow in Pictou Harbour (Figure 4-10 - Figure 4-12). During ebb tide the flow of water outside Pictou Harbour is from north to southeast, following the bathymetry contours; water in the back harbour flows northwest to exit the harbour, flowing faster in the deep channel (Figure 4-10a). Water flowing out of the main harbour channel flows to the east and southeast (Figure 4-10b), and water near the outlet of Boat Harbour flows north and then east, following the shoreline and joining the general flow pattern (Figure 4-10c). During flood tide, water enters Pictou Harbour flowing north and west from the southeast, increases in speed in the deep, narrow channel, and enters the back harbour (Figure 4-11a). The incoming tide near the outlet of Boat Harbour follows the 2 m depth contour closely, eventually flowing north to enter Pictou Harbour (Figure 4-11b). Closer to the shore near Boat Harbour water flows south towards the outlet at <0.05 m/s (Figure 4-11c).

Current speeds were highest in and near the channel, reaching 0.5 m/s along the axis of the channel; currents near the outlet of Boat Harbour were slower, approximately 0.01 m/s during maximum ebb and flood flow (Figure 4-12).

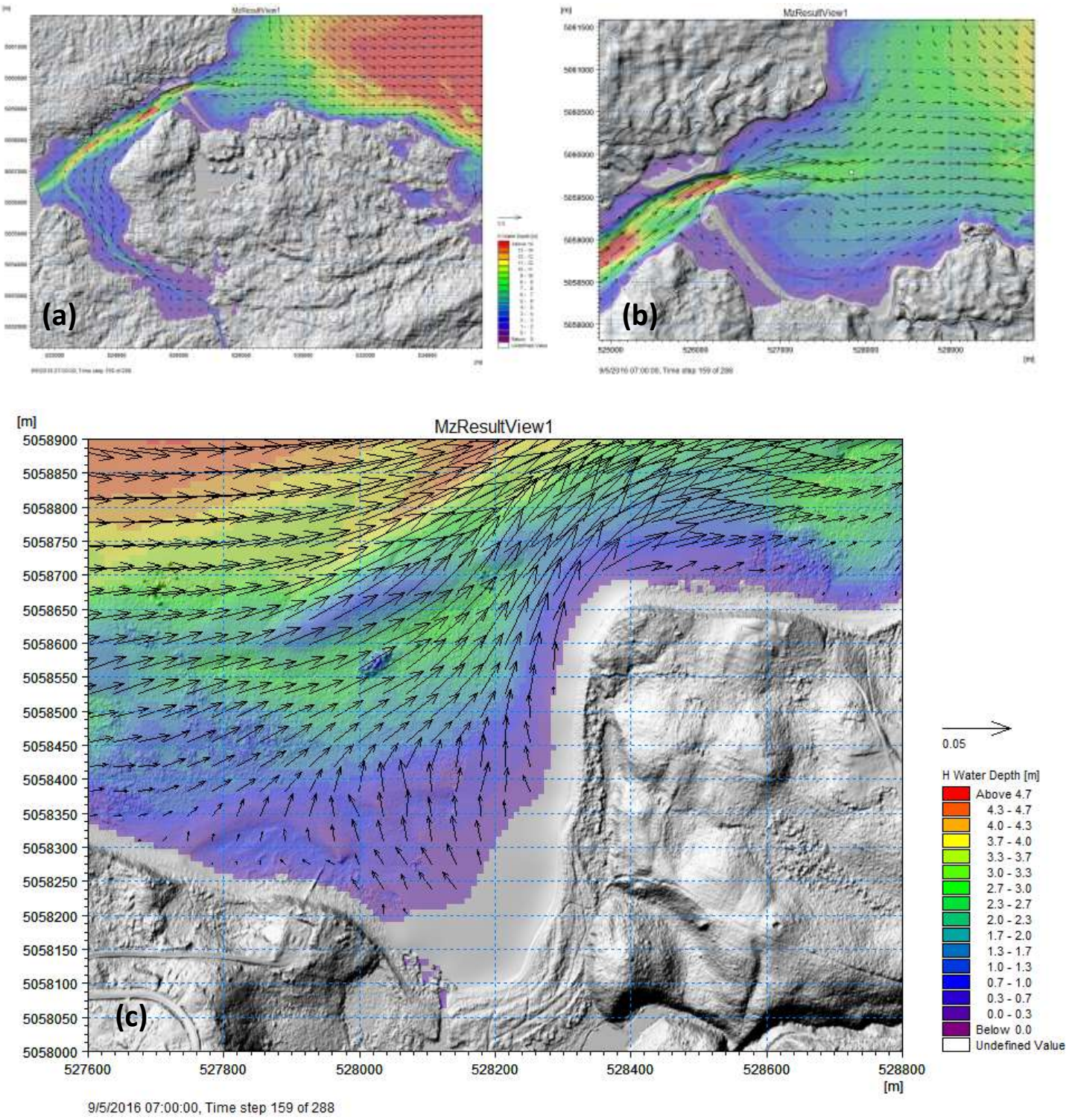

Figure 4-10: Water depth (represented by coloured contours) and velocity vectors (representing current direction and speed) during a typical flood tide (Sept. 5, 7:00). Model grid shown is (a) Domain 1, the 9 m grid, with every 35th vector plotted; (b) 9 m grid cropped to the northern lidar study area, with every 20th vector plotted; (c) 9 m grid cropped to Boat Harbour outlet, with every 4th vector plotted. Note the different vector scale for each plot, and the different colour scale for (c).

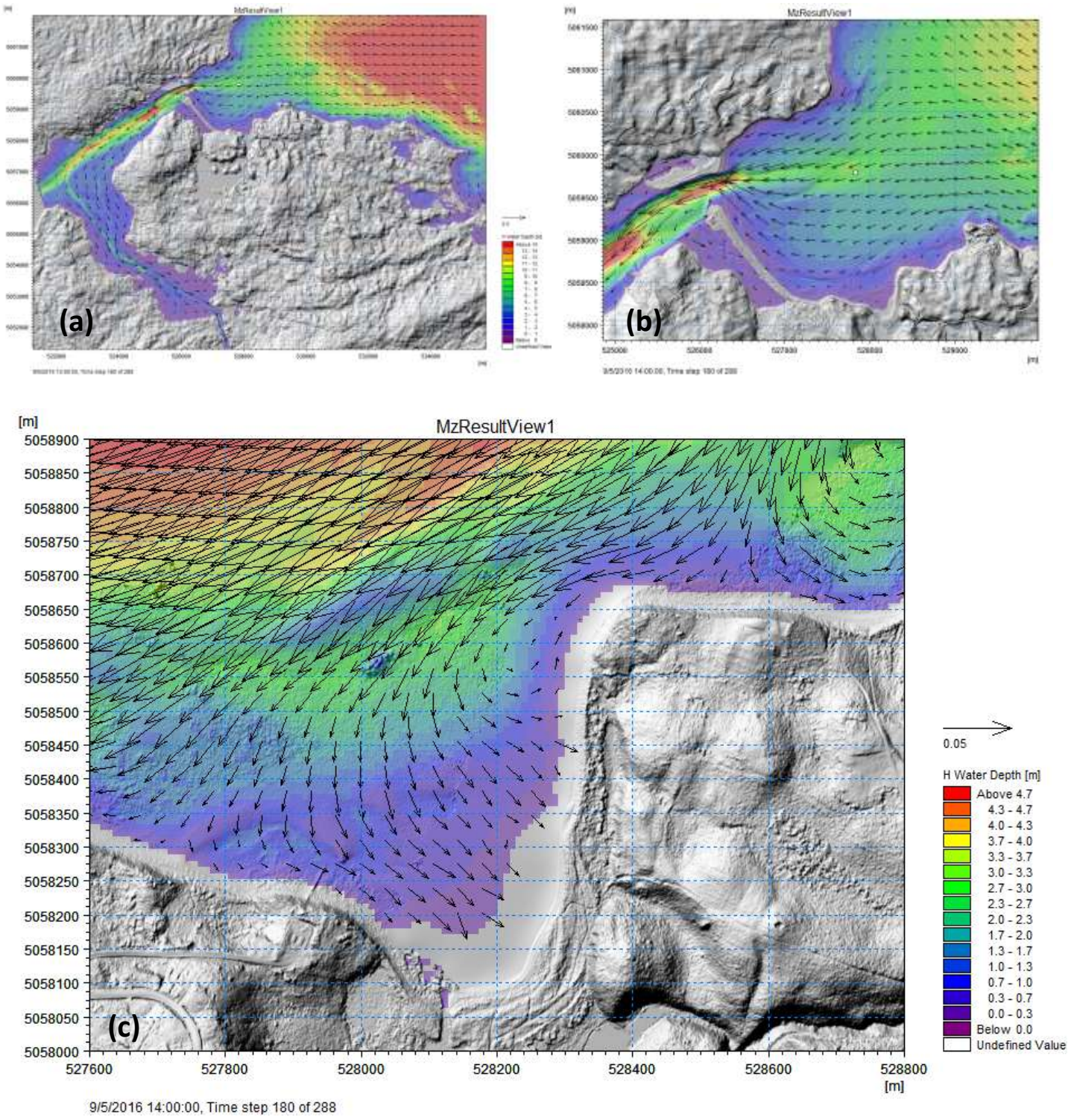

Figure 4-11: Water depth (represented by coloured contours) and velocity vectors (representing current direction and speed) during a typical ebb tide (Sept. 5, 14:00). Model grid shown is (a) Domain 1, the 9 m grid, with every 35th vector plotted; (b) 9 m grid cropped to the northern lidar study area, with every 20th vector plotted; (c) 9 m grid cropped to Boat Harbour outlet, with every 4th vector plotted. Note the different vector scale for each plot, and the different colour scale for (c).

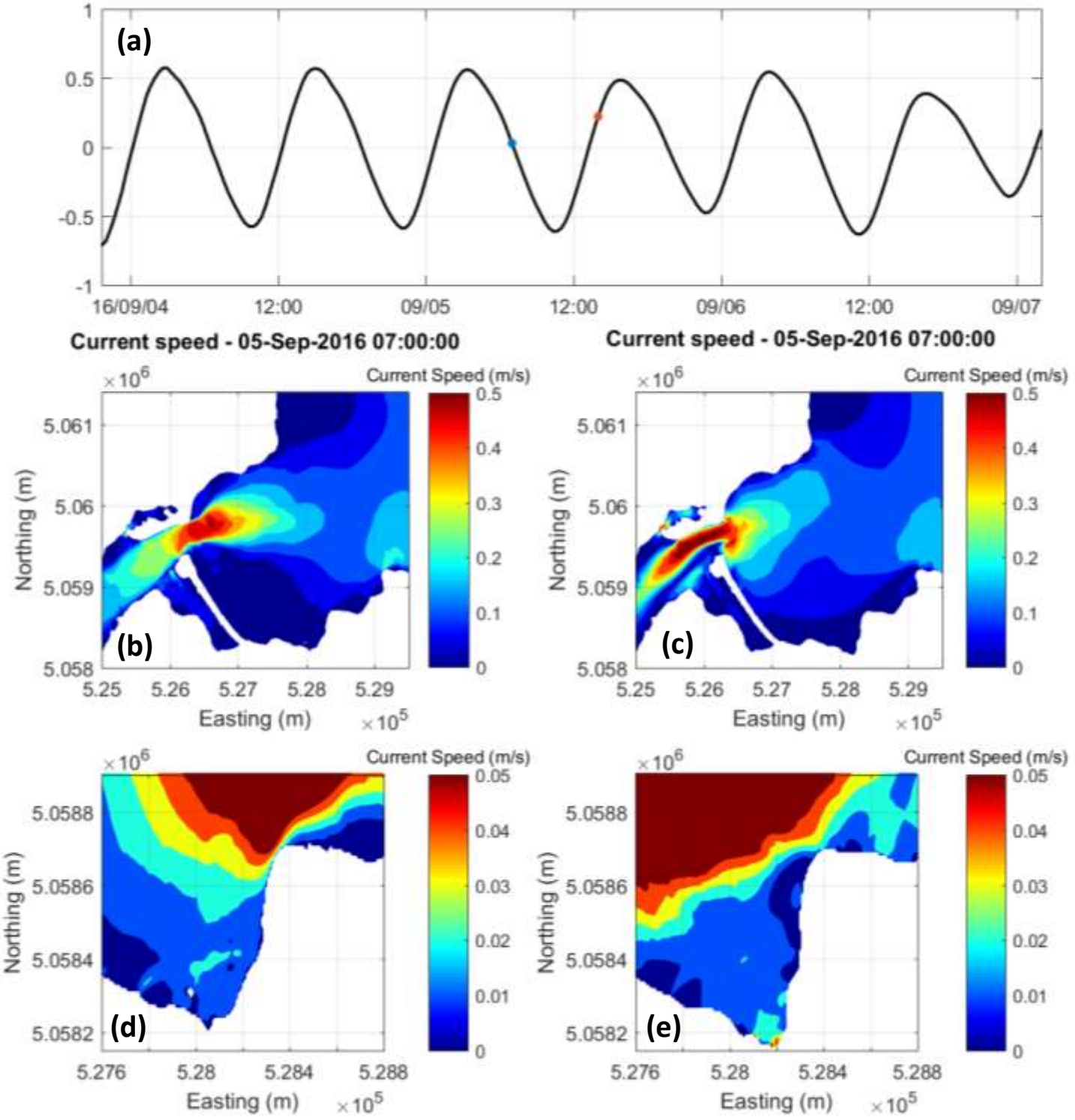

Figure 4-12: (a) Surface elevation, with markers representing the time of the lower figures. Current speeds during ebb tide (b,d) and flood tide (c,e) for the Pictou Harbour channel (b,c) and for the Boat Harbour outlet (d,e).

5 Discussion and Conclusions

A topo-bathymetric lidar survey of Pictou Harbour conducted on September 7, 2016 was successful in penetrating the seabed in the the study area, reaching a minimum elevation value of -4.8 m CGVD28. A data set from CHS consisting of 5 m multibeam data allowed the entire harbour to be covered in the study area, in particular, the channel where the lidar did not penetrate. The multibeam data were compared to the lidar in areas of overlap, along with the RTK GPS, which was validated as part of standard AGRG analysis. RTK GPS validation taken on land resulted in -0.14 m mean accuracy with a standard deviation of 0.04m, bathymetric validation resulted in -0.17 m mean accuracy with a standard deviation of 0.25 m. CHS 5m multibeam validation resulted in a -0.03 m mean with a standard deviation of 0.3 m.

Ground truth data collected by AGRG with the help of Pictou Landing First Nation in August 2016 resulted in a thorough collection throughout the study area, and were helpful in determining water clarity, bottom type and distribution of vegetation throughout the area at the time of the ground truth survey. This dataset was presented on a series of maps overlaid with the orthophoto mosaic. A seabed cover map was constructed from the aerial photos and the lidar derivatives and validated using the ground truth data.

An ADCP was deployed for 35 days to measure water level and current speeds throughout a tidal cycle. A hydrodynamic model was developed using topo-bathymetric lidar merged with the CHS multibeam data. The model was successful in simulating the current flow, water level variations and water circulation within outer Pictou Harbour and near Boat Harbour. A spatially varying bed resistance map could potentially improve model results, however, this can be implemented for future model development. Flow measurements for Pictou causeway would provide more accurate information to be used to model the flow through the causeway. The addition of wind to the model would likely not affect the overall circulation, but in future models the wind speed should be added for completeness. Ground control points for the southern portion of the study area would be useful for validating eelgrass distribution and the bottom type map for this area. The model, combined with the other data derived from this project help determine a base line condition so that in the future it can be compared when Boat Harbour is converted back to its natural setting as a tidal inlet.

6 References

DHI Water & Environment (2008). Mike 21 Flow Model Hints and Recommendations in Applications with Significant Flooding and Drying.

Dupont, F., Hannah, C.G., and Greenberg, D. (2005). Modelling the Sea Level in the Upper Bay of Fundy. Atmos-Ocean *43*, 33–47.

Varma, H., Hannah, C., MacNab, R., Costello, G., Spears, T., Woodford, W., and Delbridge, C. (2008). The Complexities in the Design and Definitions of the North West Atlantic Data Set; Searching for Rational Architecture to Implement Diverse Bathymetric Data. Proc. Can. Hydrogr. Conf. Natl. Surv. Conf.

Webster, T.L., McGuigan, K., Crowell, N., Collins, K., and MacDonald, C. (2016). Optimization of data collection and refinement of post-processing techniques for Maritime Canada's first shallow water topographic-bathymetric lidar survey. J. Coast. Res.

7 Acknowledgements

We would like to thank Public Services and Procurement Canada for funding support for this project. We would like to thank Stephen Parsons of Canadian Hydrographic Survey for providing the CHS charts and multibeam data and Pictou Landing First Nation for the assistance with the collection of ground truth data for Boat Harbour. Thanks to staff from Leica Geosystems, Leading Edge Geomatics staff for operations and AGRG staff for administrative support, the pilots from Leading Edge Geomatics.